Volatility Parameterization of Ambient Organic Aerosols at a rural site of the Northern China Plain

Siman Ren[1], Lei Yao[1], Yuwei Wang[1], Gan Yang[1], Yiliang Liu[1], Yueyang Li[1], Yiqun Lu[1], Lihong Wang[1], Lin Wang[1,2,3,4]

[1]Shanghai Key Laboratory of Atmospheric Particle Pollution and Prevention (LAP[3]), Department of Environmental Science & Engineering, Jiangwan Campus, Fudan University, Shanghai 200438, China

[2] Collaborative Innovation Center of Climate Change, Nanjing, 210023, China

[3] Shanghai Institute of Pollution Control and Ecological Security, Shanghai 200092, China

[4] IRDR International Center of Excellence on Risk Interconnectivity and Governance on Weather/Climate Extremes Impact and Public Health, Fudan University, Shanghai 200438, China

Correspondence: Lin Wang (lin_wang@fudan.edu.cn)

ABSTRACT: The volatility of organic aerosols plays a key role in determining their gas-particle partitioning, which subsequently alters the physicochemical properties and atmospheric fates of aerosol particles. Nevertheless, an accurate estimation of the volatility of organic aerosols (OA) remains challenging. Because most standards for particulate organic compounds are not available, and even for those with standards, ~~particulate organic compounds are scarce, on the other hand,~~ their vapor pressures are too low to be measured~~estimate~~ by most traditional methods. Here, we deployed an iodide-adduct Long Time-of-Flight Chemical Ionization Mass Spectrometer (LToF-CIMS) coupled with a Filter Inlet for Gases and AEROsols (FIGAERO) to probe the relationship between the molecular formula~~e~~s of atmospheric organic aerosol's components and their volatilities. A number of T_{max} (*i.e.*, the temperature corresponding to the first signal peak of thermogram) were abstracted and validated from the desorption thermograms of mixed organic and inorganic calibrants which were atomized and then collected onto a PTFE~~Teflon~~ filter. Besides, 30 filter samples of ambient air were collected in winter 2019 at Wangdu station in Beijing-Tianjin-Hebei region, and analyzed by FIGAERO-LToF-CIMS, leading to the identification of 1,448 compounds dominated by the CHO (containing carbon, hydrogen, and oxygen atoms) and CHON (containing carbon, hydrogen, oxygen, and nitrogen atoms) species. Among them, 181 organic formula~~e~~s including 91 CHO and 90 CHON compounds were then selected since their thermograms can be characterized with clear T_{max} values in more than 20 out of 30 filter samples and subsequently divided into two groups according to their O/C ratios~~.~~ and different thermal desorption behavior. The mean O/C of these two groups are 0.56 ± 0.35 (average ± one standard deviation) and 0.18 ± 0.08, respectively. ~~We T~~then ~~obtained~~ the ~~–~~ parameterizations~~correlation functions~~ between volatility and elemental composition for the two group compounds were obtained. Compared with previous volatility parameterizations, our ~~correlation~~ functions provide a better estimation ~~o~~for the volatility of ~~semi-volatility organic compounds (SVOCs) and~~ low-volatility organic compounds (LVOCs) in ~~the~~ ambient organic aerosols. Furthermore, ~~we~~ it is suggested that ~~there should be specialized~~ volatility parameterizations should be specialized for organic compounds with different O/C ratios ~~organic compounds~~.

1 Introduction

Aerosol particles can significantly impact human health, visibility and climate (Stocker et al., 2013). Organic aerosol (OA) comprises tens of thousands of organic substances and makes up a significant mass fraction of the total submicron particles in the troposphere (Jimenez et al., 2009) ~~(Nizkorodov et al., 2011)~~. Whether an organic compound will exist in the gas phase or ~~the~~ particles under a specific temperature is determined by its volatility, which depends on its molar mass and functional groups (Capouet and Müller, 2006; Pankow and Asher, 2008). The volatility of a compound is usually expressed as saturation mass concentration (C_0^*) or saturation vapor pressure (*Psat*). The effective saturation mass concentration (C^*) includes the effect of non-ideal thermodynamic mixing with an activity coefficient (γ), thus $C^* = \gamma C_0$, and C^* equals C_0 under the assumption of ideal thermodynamic mixing (Donahue et al., 2011). Saturation mass concentration is regarded as one of critical

physicochemical parameters for organic aerosols' components. The organic compounds with $C^* < 0.1\ \mu g \cdot m^{-3}$ are mostly in the condensed phase, the organic compounds with $C^* > 1000\ \mu g \cdot m^{-3}$ are almost entirely in the gas phase, and the organic compounds with $1 < C^* < 100\ \mu g \cdot m^{-3}$ will be found in both phases under typical conditions (Donahue et al., 2009). ~~(Donahue et al., 2011), and is regarded as one of the most critical physicochemical parameters for organic aerosols' components.~~

During the past years, ~~three~~ two major methods relevant to the Chemical Ionization Mass Spectrometer (CIMS) have been developed to characterize the volatility of aerosol ~~particle~~s. ~~The first one estimates the volatility of an organic compound from its partitioning between the gas phase and the particle-associated phase. Particulate fraction (F_p) for each organic compound can be calculated by measured gas phase and particle-associated concentrations or signals in the ambient atmosphere. Then F_p can be combined with the mass concentration of particulate OA, which was usually measured by an aerosol mass spectrometer (AMS) and temperature to estimate the C^* (Donahue et al., 2006; Pankow, 1994; Stark et al., 2017).~~

The ~~second~~ first one estimates the volatility of an organic species based on~~from~~ its molecular formula. The relationship between C^* and molecular formula~~e~~s of ~~seven categories of organic compounds including~~ alkane, aldehyde, ketone, alcohol, acid, diol, and diacid was proposed by ~~(~~Donahue et al.~~,~~ (2011), ~~based on a group contribution method SIMPOL (Pankow and Asher, 2008),~~ which clarifies the relationship between n_C (the numbers of carbon) and n_O (the numbers of oxygen), and logC_0. The relationship was derived from a group contribution method SIMPOL that actually is a structure-based estimation method (Pankow and Asher, 2008) ~~(C^* equals C_0 under the assumption of ideal thermodynamic mixing) (Donahue et al., 2011).~~ Li et al. (-2016) updated this function by including 31066 compounds from the National Cancer Institute (NCI) open database, which applies to not only CHO compounds (containing carbon, hydrogen, and oxygen atoms) but also the nitrogen- and sulfur-containing ~~N- and S-containing~~ compounds. However, Isaacman-Vanwertz and Aumont. (2021) showed that the volatility of CHON compounds estimated by the Li et al. (2016) parameterization is significantly biased by an increase in the number of nitrogen atoms, and thus they modified the nitrogen coefficient for CHON compounds from Li et al. (2016) study by using a fixed relationship between the nitrogen coefficient and the number of the oxygen atom (*i.e.*, b_N=-2*b_O). – On the other hand, Donahue et al. (2011) took only -OH, =O and -C(O)OH functionalities into account when describing an average effect of an added oxygen, which could result in a large uncertainty when estimating the volatility of highly oxygenated organic molecules (HOMs) that contain hydroperoxide (-OOH) functionalities. Thus, Stolzenburg et al. (~~Stolzenburg et al.,~~ 2018) and Mohr et al. (-2019) updated the parameters for the volatility estimation of HOMs, based on 15 HOMs. –The molecular structures of these 15 HOMs are unclear, but their saturation concentrations were estimated using the SIMPOL method on the basis of supposed molecular structures~~with known molecular structures and saturation concentrations~~ (Tröstl et al., 2016). ~~In addition,~~ A~~a~~s the covalently bonded dimers are abundant in HOMs from ozonolysis of α-pinene, Stolzenburg et al. (2018) fitted parameters using monomer and dimer HOMs separately, allowing a parameter to include the covalent binding~~the covalent binding to be an independent parameter~~. Since molecular formula~~e~~s of organic aerosols can be obtained by state-of-the-art instruments such as high-resolution mass spectrometers, C^* of organic compounds in the aerosol particles can then be calculated based on the above-mentioned empirical function (Huang et al., 2019).

The ~~third~~ second one estimates the volatility of an organic species on the basis of~~from~~ its desorption thermogram. When analyzing physicochemical properties of aerosol particles, one of the most popular techniques is to heat the particles and then detect the evaporated compounds utilizing mass spectrometry techniques, such as Thermodenuder-particle Beam Mass Spectrometer (Faulhaber et al., 2009), Thermal-Desorption Chemical Ionization Mass Spectrometer (TD-CIMS) (Smith et al., 2004), Micro-Orifice Volatilization Impactor Coupled to a Chemical Ionization Mass Spectrometer (MOVI-CIMS) (Yatavelli and Thornton, 2010), Chemical Analysis of Aerosols Online -Proton Transfer Reaction Mass Spectrometer (CHARON-PTR-MS) (Eichler et al., 2015), and the Filter Inlet for Gases and AEROsols (FIGAERO) coupled with Time-of-Flight Chemical Ionization Mass Spectrometer (ToF-CIMS) (Lopez-Hilfiker et al., 2014). Basically, the desorption temperature is ramped up linearly, the particulate organic compounds with different vapor pressures are thermo-desorbed and then characterized with distinct thermograms (*i.e.*, desorption signal versus temperature~~the evolution of mass spectral signals in a range of desorption~~

~~temperatures~~), and the temperature corresponding to the first peak signal (T_{max}) correlates with the vaporization enthalpy of a compound (Lopez-Hilfiker et al., 2014). It is thus applicable to estimate C^*, *i.e.*, the volatility of the chemical constituents in the particles, from the measured T_{max}, after calibration with a set of standards with known vapor pressures (Bannan et al., 2019), which has been widely applied in many previous studies (Nah et al., 2019; Stark et al., 2017; Wang et al., 2020a; Ye et al., 2019; Ylisirniö et al., 2019). Compared with the parameterization method from organic aerosols' molecular formula~~es~~, the thermogram method is able to give a volatility distribution that is likely closer to the real one.~~,~~ S~~s~~ince the molecular formula method likely treats the thermal decomposition products after heating as evaporated organic molecules ~~after heating~~, and thus overestimate~~sd~~ the overall volatility of a group of organics (Stark et al., 2017).

The FIGAERO-ToF-CIMS has been widely used in the field and laboratory studies in recent years. For example, Wang et al. (2020a) explored the volatility of aromatic hydrocarbon photo-oxidation products, Ylisirniö et al. (2020~~19~~) compared the volatility of SOA (Secondary Organic Aerosol) components formed from oxidation of real tree emissions with that formed from oxidation of single VOC-systems, and Ye et al. (2019) studied the volatility of nucleated particles from α-Pinene oxidation between -50 ˚C and +25 ˚C using FIGAERO-ToF-CIMS. ~~The success of this method depends on~~ Accurately measuring ~~whether or not~~ the desorption thermograms of the standards ~~are accurately measured~~is one of the essential factors for the success of this method~~, which is yet under discussion~~. For example, previous studies typically used the syringe deposition method to prepare the mimic filter, which leads to wide variations in results. A new method for volatility calibration, the atomization method, accurately captures the evaporation of chemical constituents from ambient aerosol particles (Ylisirniö et al., 2021). In addition, the influences of mixing of organic compounds and inorganic salts that are a major component in ambient aerosol particles on the thermograms of organics, were~~was~~ not considered in these previous studies.

On the other hand, with rapid economic growth and urbanization in the North China Plain (NCP), air pollution and extreme haze events frequently occurred in this region, the formation of which is closely related to the volatility of aerosol components (Li et al., 2017; Shiraiwa and Seinfeld, 2012). ~~Volatility may also have an impact on the air pollution and haze events in this region.~~ Therefore, it is crucial to understand the volatility of aerosol components in the NCP.

In this study, we compared the effects of the methods of syringe deposition and atomization on T_{max} with a series of authentic organic standards using FIGAERO-LToF-CIMS. Also, we investigated the influences of inorganic salts and the mixing of organic compounds on the T_{max} of organics. In addition, we developed empirical volatility-molecular formula functions based on ~~measured C^* of~~ selected CHO and CHON compounds with varying~~ious~~ O/C ratios ~~in~~ from ambient OA particles. The C^* of these selected compounds were estimated by obtained T_{max} from thermograms.~~,~~ ~~which~~ The ambient particles were collected at Wangdu station in the North China Plain, China, from January 15 to 22, 2019. Besides, o~~O~~ur empirical functions were also compared with previous ones.

2 Experimental methods

2.1 FIGAERO-LToF-CIMS

We measured the chemical composition and thermograms of particulate compounds collected on filters via a FIGAERO-LToF-CIMS with a mass resolving power of 7700-8500, and the volatility of compounds was acquired from thermograms (Bertram et al., 2011; Lee et al., 2014; Lopez-Hilfiker et al., 2014). The design and operation of the FIGAERO have been introduced in previous studies (Bannan et al., 2019; Lopez-Hilfiker et al., 2014; Thornton et al., 2020; Ye et al., 2020). In this study, particles collected in the lab calibration experiments or from the field campaign were thermally desorbed utilizing an ultrahigh purity (UHP) nitrogen flow at 2.3 Liter per minute^{-1} (lpm), among which 1.0 lpm U~~P~~HP N_2 passed the filter and entered the ion-molecule reaction (IMR) chamber. In IMR, organic molecules were charged by iodide ions generated by ~~the~~ exposure of a 1.0 lpm ~~the~~ mixture of CH_3I and ~~–~~UHP N_2 to a 0.1 mCi radioactive Am-241 source. During the thermo-desorption process, the heating temperature ramp linearly started ~~roughly~~ from room temperature (~25 ˚C) to 134 ˚C and then the filter was held at 134 °C for 40 min to ensure that most of the organic compounds had been desorbed from the filter (Lopez-Hilfiker et al., 2016).

The measured ramping rate for heating was 2.27 ˚C /min in this study. A slower ramping rate allows more time to stay at any momentary desorption temperature so that a larger fraction of molecules would evaporate. Also, a slower ramping rate can separate compounds with similar volatilities better and lead to a smaller number of thermal decomposition products (Lopez-Hilfiker et al., 2014; Yang et al., 2021; Ylisirniö et al., 2021). Most of the ambient organic compounds can be desorbed from the filter at less than 134 °C (Huang et al., 2019). Furthermore, high molecular weight organic compounds (e.g. $C_{27}H_{52}O_4$) can be evaporated from the filter below 120 °C (Wang et al., 2016). Therefore, the highest temperature of 134 ˚C is feasible in our study. –The desorption procedure for the calibration experiments and the field measurements were the same, as shown in Figure S1. During –ambient filter measurements, background measurements using a blank filter were also conducted. The blank filter was analyzed by the same thermal desorption procedure as that of the field samples. The obtained signals are treated as the background signals. An example of the background signal of an identified compound was shown in Figure S2~~1~~.

A Tofware software (version 3.1.2, Tofwerk AG, Switzerland) was used to analyze the data of the mass spectrometer. To plot thermograms, signals of evaporated compounds were normalized by the abundance of ~~the~~ reagent ions and then subtracted with the background signals, which were normalized similarly. The raw data was acquired at a frequency of 1 Hz and then averaged to a 20 s time interval during the data analysis. As the desorption features of ambient aerosol particles were quite complex, we applied the Levenberg–Marquardt algorithm to fit the thermograms and conducted peak deconvolution for the multimodal thermograms (Goodman and Brenna, 1994; Lopez-Hilfiker et al., 2015; Stolzenburg et al., 2018). In the case of a multimodal thermogram, the higher-temperature peak(s) (*i.e.*, the warmer peak) was assumed to come from the thermal decomposition of larger molecules or isomers with different vapor pressures (Huang et al., 2018; Wang et al., 2016)~~,~~. H~~h~~ence, in this study, T_{max} of the cooler peak (*i.e.*, the first peak) was used to estimate the volatility of an organic compound.

2.2 Calibration experiments

The C^* versus T_{max} calibration curve was obtained by species with known vapor pressures. Two methods referred as the syringe deposition method and the atomization method, were used to prepare filter samples of authentic compounds. For the syringe deposition method, certain amounts of authentic species dissolved in the acetonitrile solvent were injected onto a PTFE filter by a syringe. While the acetonitrile solvent was supposed to quickly evaporate from the filter and have a minor effect on authentic species, only the authentic species were thermally desorbed during the subsequent FIGAERO-LToF-CIMS analysis. For the atomization method, the authentic species dissolved in deionized water were atomized by a commercial atomizer (TSI® 3076). Atomized particles were diluted and dried by a zero-gas flow and silica gel ~~tubes~~, after which the relative humidity (RH) of the flow was regulated to around ~~-~~2% (Figure S3~~2~~). Then, particles were collected onto a PTFE filter and subsequently analyzed by the FIGAERO-LToF-CIMS. The mass ~~amount~~ of collected particles can be calculated based on the number size distribution of particles measured by a Scanning Mobility Particle Sizer (SMPS, TSI® 3776), the particle density, the collection time, and the flow rate through the filter (Ylisirniö et al., 2021). Among them, the particle density can be estimated according to the density of corresponding authentic standards and their mixing ratios in the solution.

During our laboratory tests, eleven~~five~~ sets of calibration experiments were conducted. These experiment conditions are summarized in Table 1. One set of (No.1) experiments using the syringe deposition method were performed, where polyethylene glycols (PEGs) were used as authentic organic standards (Bannan et al., 2019). Besides, ~~four~~ ten sets of atomization experiments were also conducted. The ~~second (~~No.2~~)~~ set works as an intercomparison with previous syringe deposition (No.1) experiments. The ~~third, fourth and fifth (~~No.3-7~~5)~~ set~~s of~~ experiments were conducted ~~in order~~ to explore the effect~~s~~ of ammonium sulfate and mixed organic compounds on the T_{max} of organics. ~~In these three sets,~~ Eerythritol, PEG-6, PEG-7, PEG-8, and citric acid were used as authentic organic standards because they can co-dissolve with ammonium sulfate in deionized water. In ~~the third (~~No.3~~) set~~, ammonium sulfate was not added to the standard solution, and there were only organic standards. In ~~the fourth (~~No.4~~)~~ and No.5~~ set~~, ammonium sulfate was mixed with erythritol, PEG-6, PEG-7, PEG-8, and citric acid, respectively. 200 ng and 1000 ng atomized particles were collected in No.4 and No.5, respectively. It is assumed that the atomized particles were internally mixed with the same mass ratio as that in the solution (Drisdell et al., 2009), consisting of 100 ng/500 ng of ammonium sulfate and 100 ng/500 ng of the mixed organic standard. Although

ammonium sulfate is much less volatile than mixed organics and the mixing ratio of ammonium sulfate to organic compounds in atomized particles might be different with that in solution, this assumption likely leads to a minor effect on the matrix effect of ammonium sulfate. –In the sixth (No.6) set, erythritol, PEG-6, PEG-7, PEG-8, and citric acid were mixed together and 1000 ng atomized particles were collected. In ~~the fifth (~~No.7~~5) set~~, ammonium sulfate was mixed with erythritol, PEG-6, PEG-7, PEG-8, and citric acid ~~together. 1000 ng atomized particles were collected. With the same assumption as mentioned above, the particles consisted of 500 ng of ammonium sulfate and 100 ng of each organic standard~~ .The No.7-11 sets of experiments were conducted to explore the effect of mass loading of filters. –Four replicates were performed for each set of experiments.

Table 1. Conditions of eleven~~five~~ sets of calibration experiments.

No.	Method	Authentic standards	Concentration	Solvent	Deposited volume	Mass loading
1	Syringe deposition	PEG-4 ($C_8H_{18}O_5$) PEG-5 ($C_{10}H_{22}O_6$) PEG-6 ($C_{12}H_{26}O_7$) PEG-7 ($C_{14}H_{30}O_8$) PEG-8 ($C_{16}H_{34}O_9$)	0.05 g L^{-1} 0.05 g L^{-1} 0.05 g L^{-1} 0.05 g L^{-1} 0.05 g L^{-1}	Acetonitrile	2 μl	100 ng 100 ng 100 ng 100 ng 100 ng~~100 ng~~
2	Atomization	PEG-4 ($C_8H_{18}O_5$) PEG-5 ($C_{10}H_{22}O_6$) PEG-6 ($C_{12}H_{26}O_7$) PEG-7 ($C_{14}H_{30}O_8$) PEG-8 ($C_{16}H_{34}O_9$)	1.0 g L^{-1} 1.0 g L^{-1} 1.0 g L^{-1} 1.0 g L^{-1} 1.0 g L^{-1}	Deionized water	/	500 ng 500 ng 500 ng 500 ng 500 ng~~500 ng~~
3	Atomization	Erythritol ($C_4H_{10}O_4$) PEG-6 ($C_{12}H_{26}O_7$) PEG-7 ($C_{14}H_{30}O_8$) PEG-8 ($C_{16}H_{34}O_9$) Citric acid ($C_6H_8O_7$)	0.5 g L^{-1} 0.5 g L^{-1} 0.5 g L^{-1} 0.5 g L^{-1} 0.5 g L^{-1}	Deionized water	/	100 ng 100 ng 100 ng 100 ng 100 ng~~100 ng~~
4	Atomization	Erythritol ($C_4H_{10}O_4$) +ammonium sulfate PEG-6 ($C_{12}H_{26}O_7$) + ammonium sulfate PEG-7 ($C_{14}H_{30}O_8$) + ammonium sulfate PEG-8 ($C_{16}H_{34}O_9$) + ammonium sulfate Citric acid ($C_6H_8O_7$) + ammonium sulfate	0.5 g L^{-1} + 0.5 g L^{-1} 0.5 g L^{-1} + 0.5 g L^{-1} 0.5 g L^{-1} + 0.5 g L^{-1} 0.5 g L^{-1} + 0.5 g L^{-1} 0.5 g L^{-1} + 0.5 g L^{-1}	Deionized water	/	200 ng (100 ng + 100 ng) 200 ng (100 ng + 100 ng) 200 ng (100 ng + 100 ng) 200 ng (100 ng + 100 ng) 200 ng (100 ng + 100 ng)
5	Atomization	Erythritol ($C_4H_{10}O_4$) +ammonium sulfate PEG-6 ($C_{12}H_{26}O_7$) + ammonium sulfate PEG-7 ($C_{14}H_{30}O_8$) + ammonium sulfate PEG-8 ($C_{16}H_{34}O_9$) + ammonium sulfate Citric acid ($C_6H_8O_7$) + ammonium sulfate	0.5 g L^{-1} + 0.5 g L^{-1} 0.5 g L^{-1} + 0.5 g L^{-1} 0.5 g L^{-1} + 0.5 g L^{-1} 0.5 g L^{-1} + 0.5 g L^{-1} 0.5 g L^{-1} + 0.5 g L^{-1}	Deionized water	/	1000 ng (500 ng + 500 ng) 1000 ng (500 ng + 500 ng) 1000 ng (500 ng + 500 ng) 1000 ng (500 ng + 500 ng) 1000 ng (500 ng + 500 ng)
6	Atomization	Erythritol ($C_4H_{10}O_4$) + PEG-6 ($C_{12}H_{26}O_7$) +PEG-7 ($C_{14}H_{30}O_8$) + PEG-8 ($C_{16}H_{34}O_9$) + citric acid ($C_6H_8O_7$)	0.5 g L^{-1} + 0.5 g L^{-1} +0.5 g L^{-1} + 0.5 g L^{-1} +0.5 g L^{-1}	Deionized water	/	1000 ng (200 ng + 200 ng +200 ng +200 ng + 200 ng)
~~5~~7	Atomization	Erythritol ($C_4H_{10}O_4$) + PEG-6 ($C_{12}H_{26}O_7$) + PEG-7 ($C_{14}H_{30}O_8$) + PEG-8 ($C_{16}H_{34}O_9$) + citric acid ($C_6H_8O_7$) + ammonium sulfate	0.5 g L^{-1} + 0.5 g L^{-1} +0.5 g L^{-1} + 0.5 g L^{-1} +0.5 g L^{-1} + 2.5 g L^{-1}	Deionized water	/	1000 ng (100 ng + 100 ng +100 ng +100 ng + 100 ng + 500 ng)
8	Atomization	Erythritol ($C_4H_{10}O_4$) + PEG-6 ($C_{12}H_{26}O_7$) + PEG-7 ($C_{14}H_{30}O_8$) + PEG-8 ($C_{16}H_{34}O_9$) + citric acid ($C_6H_8O_7$) + ammonium sulfate	0.5 g L^{-1} + 0.5 g L^{-1} +0.5 g L^{-1} + 0.5 g L^{-1} +0.5 g L^{-1} + 2.5 g L^{-1}	Deionized water	/	200 ng (20 ng + 20 ng +20 ng +20 ng + 20 ng + 100 ng)
9	Atomization	Erythritol ($C_4H_{10}O_4$) + PEG-6 ($C_{12}H_{26}O_7$) + PEG-7 ($C_{14}H_{30}O_8$) + PEG-8 ($C_{16}H_{34}O_9$) + citric acid ($C_6H_8O_7$) + ammonium sulfate	0.5 g L^{-1} + 0.5 g L^{-1} +0.5 g L^{-1} + 0.5 g L^{-1} +0.5 g L^{-1} + 2.5 g L^{-1}	Deionized water	/	500 ng (50 ng + 50 ng +50 ng +50 ng + 50 ng + 250 ng)
10	Atomization	Erythritol ($C_4H_{10}O_4$) + PEG-6 ($C_{12}H_{26}O_7$) + PEG-7 ($C_{14}H_{30}O_8$) + PEG-8 ($C_{16}H_{34}O_9$) + citric acid ($C_6H_8O_7$) + ammonium sulfate	0.5 g L^{-1} + 0.5 g L^{-1} +0.5 g L^{-1} + 0.5 g L^{-1} +0.5 g L^{-1} + 2.5 g L^{-1}	Deionized water	/	1500 ng (150 ng + 150 ng +150 ng +150 ng + 150 ng + 750 ng)

11	Atomization	Erythritol ($C_4H_{10}O_4$) + PEG-6 ($C_{12}H_{26}O_7$) + PEG-7 ($C_{14}H_{30}O_8$) + PEG-8 ($C_{16}H_{34}O_9$) + citric acid ($C_6H_8O_7$) + ammonium sulfate	0.5 g L^{-1} + 0.5 g L^{-1} +0.5 g L^{-1} + 0.5 g L^{-1} +0.5 g L^{-1} + 2.5 g L^{-1}	Deionized water	/	2000 ng (200 ng + 200 ng +200 ng +200 ng + 200 ng + 1000 ng)

2.3 Field Campaign

An ambient campaign was conducted from December 16, 2018 to January 22, 2019 at Wangdu station, Hebei Province, China (Wang et al., 2020b). The campaign site (38.66 °N, 115.19 °E) was mainly influenced by the surrounding transportation, industrial and residential sources, and farmlands and forests and can be treated as a typical suburban station.

Aerosol particles ($PM_{2.5}$) were collected four times every day, and each collection lasted for 15 minutes (*i.e.*, 7:00-7:15, 12:00-12:15, 17:30-17:45, and 21:00-21:15 local time, respectively). Ambient $PM_{2.5}$ was sampled onto PTFE filters (5 μm pore size, 25 mm diameter, Millipore), and the flow rate was regulated at 1.42 L min^{-1}. After the collection, filter samples were preserved at -20 ˚C in a freezer until further analysis. In this study, 30 filter samples between January 15, 2019 and January 22, 2019 were analyzed with FIGAERO offline, because mass loadings of these 30 filter samples varied from 200 ng to 3500 ng with a median of 1100 ng, which is similar to those in the calibration experiments. The mass concentration of $PM_{2.5}$ was also measured by a commercial synchronized hybrid real-time particulate monitor (TEI, Model 5030i).

2.4 Saturation mass concentration (*C**)

2.4.1 Calculation of *C**

By correlating the logarithm of P_{sat} at 298K of these authentic standards in the literature to their T_{max} values obtained from the desorption thermograms, a linear relationship can be obtained (Bannan et al., 2019):

$$log_{10}(P_{sat}) = aT_{max} + b, \quad (1)$$

where a and b are fitted parameters, and this expression can also be expressed as:

$$P_{Sat}(pa) = 10^{aT_{max}+b}, \quad (2)$$

On the other hand, P_{sat} can be converted to C^* with the assumption of the ideal gas law (Ylisirniö et al., 2020, 2021) ~~(Ylisirniö et al., 2019, 2021)~~. In this way, the relationship between C^* and T_{max} was deduced as:

$$C^*\ (\mu g \cdot m^{-3}) = \frac{(10^{aT_{max}+b})M_w}{RT}10^6, \quad (3)$$

where M_w is the molecular weight of an authentic compound (g mol^{-1}), R is the gas constant (8.314 J mol^{-1} K^{-1}), and T is the temperature when the P_{sat} is determined (K; in our study, T is 298 K).

2.4.2 Correlation between *C** and molecular formula~~e~~s

We substituted the measured T_{max} of selected organic compounds in the ambient aerosol particles into Eq. (3) with fitted a and b values from experiments with authentic standards, and obtained their C^*. Then we correlated C^* to molecular formula~~e~~s of these selected organic compounds in a function similar to what was developed in a previous study (Donahue et al., 2011; Mohr et al., 2019) :

$$log_{10}\,C_0 = (n_c^0 - n_c)b_c - (n_o - 3n_N)b_o - 2\cdot\frac{(n_o - 3n_N)n_c}{(n_c + n_o - 3n_N)}b_{co} - n_N b_N \quad (4)$$

where n_c^0 is the reference carbon number and set to be 25 (Donahue et al., 2011); n_c, n_o and n_N is numbers of carbon, oxygen and nitrogen atoms in an organic species, respectively; b_c, b_o and b_N denotes the contribution of each kind of atoms to $log_{10}\,C_0$, respectively, and b_{co} is the carbon-oxygen nonideality (Donahue et al., 2011; Li et al., 2016). Values of b_c, b_o, b_N, and b_{co} were fitted with multi-linear least-squares analysis.

3 Results and discussion

3.1 Laboratory Calibration

~~Figure 1 (and~~ Figure S~~43)~~ compares the T_{max} values for the same authentic organic standards when using different calibration methods. PEG4 was not detected by CIMS with the second (No.2) set of calibration experiments, which is consistent with the result of a previous study (Ylisirniö et al., 2021). This observation is most likely due to the high volatility of PEG-4 that leads to its evaporation even before the CIMS measurement (Ylisirniö et al., 2021). The T_{max} values measured with the syringe deposition experiments have larger error bars (Figure S4). The T_{max} may increase with increased filter loadings (Wang and Hildebrandt Ruiz, 2018), if calibrated with the same method. However, despite a larger mass loading (500 ng) in the atomization (No.2) experiments than that (100 ng) in the syringe deposition (No.1) experiments, the T_{max} values measured with the atomization method is about 20 ˚C lower than those with the syringe deposition method for the same compound. This observation can be explained by the fact that the surface area of the material deposited by the syringe is smaller than that of deposited aerosol particles, which requires more time to evaporate and correspond to higher T_{max} values (Ylisirniö et al., 2021).

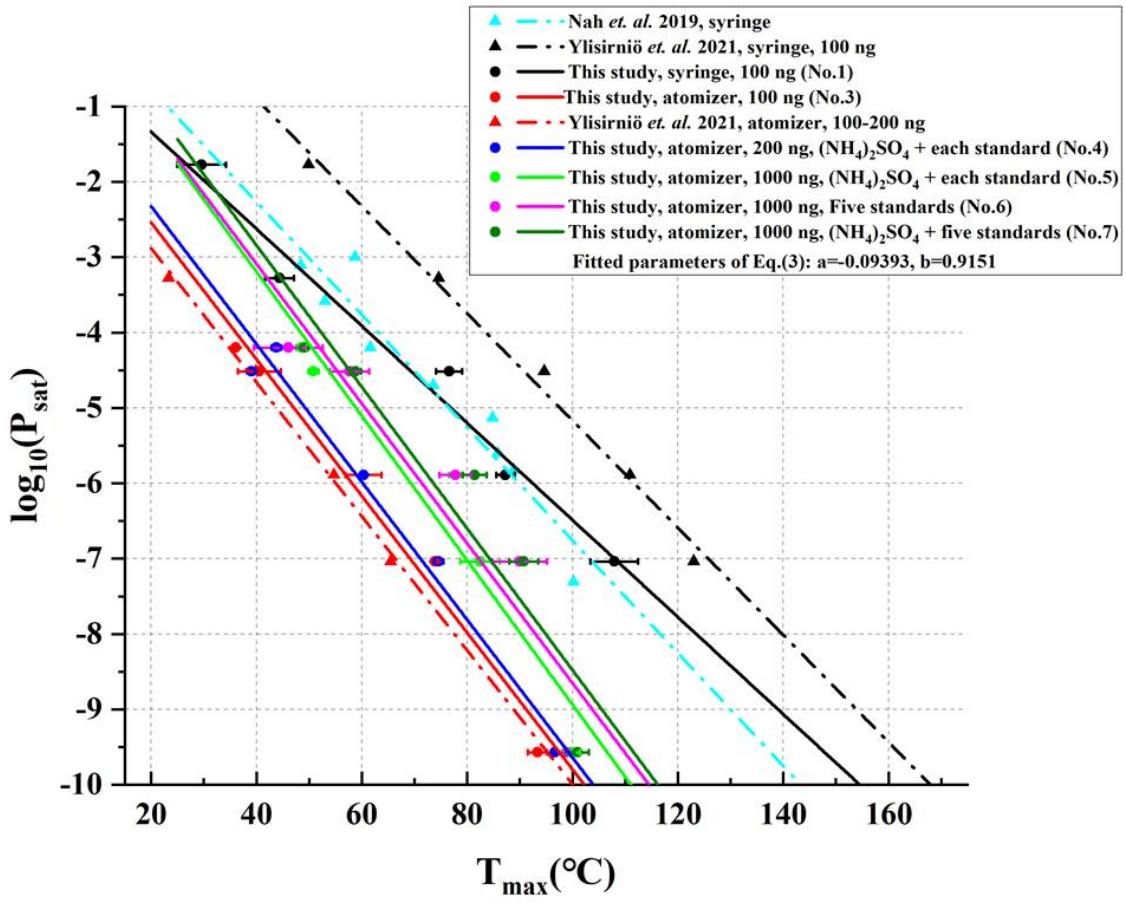

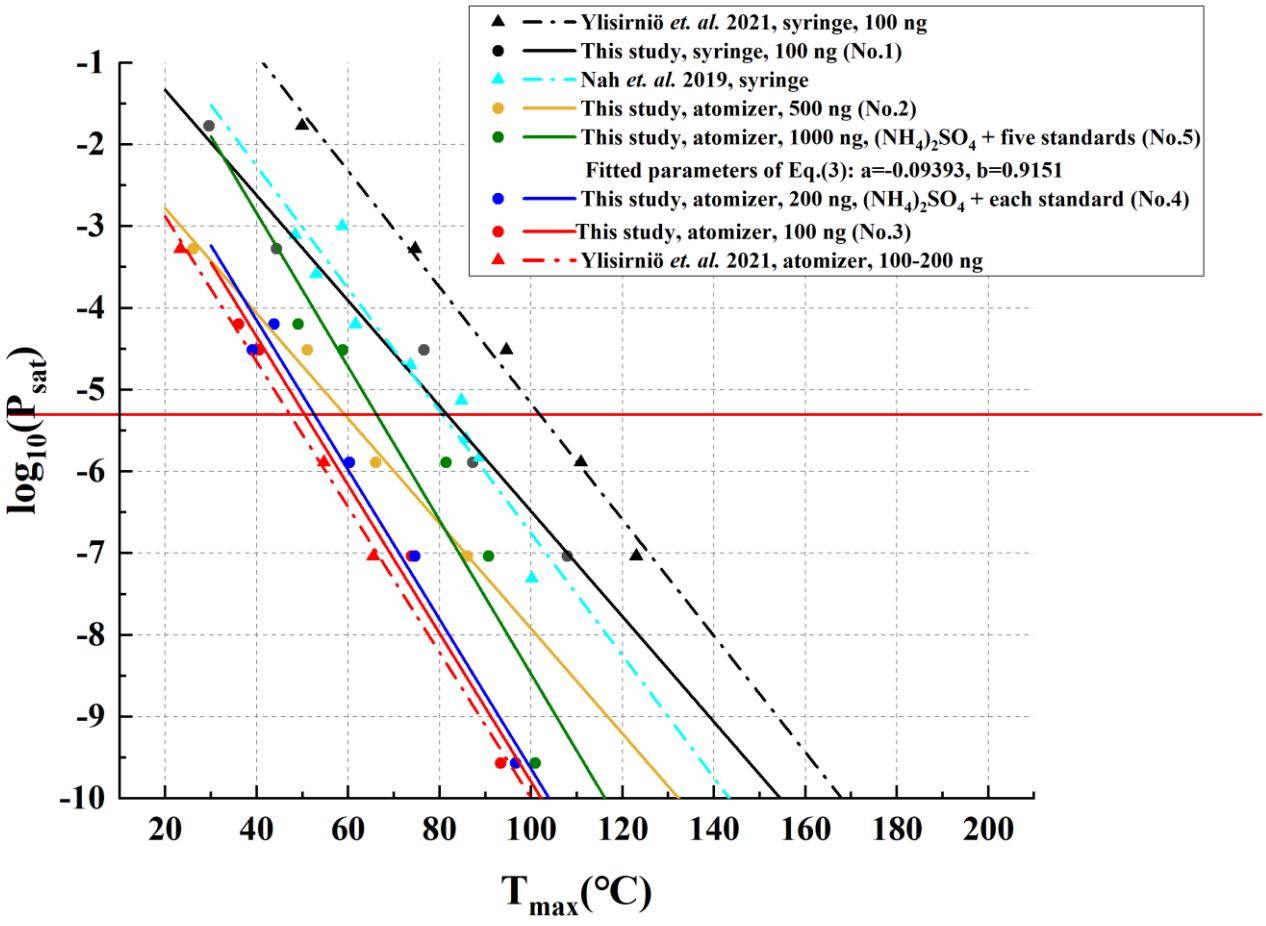

Figure 1. Comparison of calibration results obtained in this study with those reported previously. These solid lines denote the calibration results obtained in this study. Error bars represent ± one standard deviation of T_{max} from four replicate experiments. ~~The solid black line denotes the calibration results obtained with 100 ng deposited PEGs (including PEG-4, PEG-5, PEG-6, PEG-7 and PEG-8) in this study by the syringe method. The solid orange line denotes calibration results obtained with 500 ng deposited PEGs (including PEG-4, PEG-5, PEG-6, PEG-7 and PEG-8) in this study by the atomization method. The solid red line denotes calibration results in the absence of ammonium sulfate obtained with 100 ng deposited erythritol, PEG-6, PEG-7, PEG-8, and citric acid in this study using the atomization method. The solid blue line denotes calibration results obtained by adding ammonium sulfate to erythritol, PEG-6, PEG-7, PEG-8, and citric acid, respectively, in this study using the atomization method, and 200 ng dried particles were collected. The solid green line denotes calibration results for the mixture of ammonium sulfate, erythritol, PEG-6, PEG-7, PEG-8, and citric acid obtained in this study using the atomization method, and 1000 ng dried particles were collected.~~ –The light blue dash-dot line denotes calibration results obtained with acids and erythritol by Nah et al.~~,~~ (2019) using the syringe method. The black dash-dot line represents calibration results obtained with 100 ng deposited PEGs (including PEG-4, PEG-5, PEG-6, PEG-7, and PEG-8) by Ylisirniö et al.~~,~~ (2021) using the syringe method. The red dash-dot line denotes calibration results obtained with 100-200 ng ~~deposited~~ PEGs (including PEG-5, PEG-6, PEG-7, and PEG-8) by Ylisirniö et al.~~,~~ (2021) using the atomization method.

In Figure 1, we further compared our calibration results with previously reported ones. Six~~Five~~ solid calibration lines acquired in this study are located between the dash-dot calibration lines by Ylisirniö et al. (2021) using the atomization method and the syringe deposition method. The solid calibration line obtained with PEGs (O/C > 0.25) by the syringe deposition method in this study is quite close~~similar~~ to the dash-dot calibration line that was also obtained by the syringe deposition method~~, but~~ with acids (~~including acid with~~ O/C < 0.25 and O/C > 0.25) and erythritol (O/C > 0.25) (Nah et al., 2019)~~(Rao and Vejerano, 2018).~~ Yet the slopes of two lines are a bit different, which may be attributed to different O/C ratio of organic standards. ~~which~~

~~hints authentic organic standards may have less effect on the calibration line.~~ In addition, the calibration line obtained with 100 ng deposited standards in this study by the atomization method almost overlaps that obtained with the same method, standard, and mass loading (Ylisirniö et al., 2021). However, the calibration line obtained with 100 ng deposited standards in this study by the syringe deposition method is far away from the dash-dot calibration line obtained with the same method, standard, and mass loading (Ylisirniö et al., 2021). Clearly, compared with the syringe deposition method, the atomization method shows much better repeatability, even between different studies.

The effects of ammonium sulfate and mixed organic compounds ~~–~~on T_{max} of organics are~~is~~ also investigated, as shown in Figure 1 ~~(~~and Figure S5~~4)~~, since the majority of atmospheric aerosol particles consists of ~50% ammonium sulfate and 50% carbonaceous components (Drisdell et al., 2009). Clearly, ~~–~~mixing the same amount of ammonium sulfate with each of the five organic standards, as done in ~~the fourth (~~No.4~~) set of calibration experiments~~, increased the T_{max} values of erythritol and citric acid but did not alter the T_{max} values of PEGs 6-8 significantly. Comparison of the T_{max} values of No.6 and No.7 showed that the T_{max} of five organics exhibited a slight increase (1 to 4 ℃), which is likely due to the addition of ammonium sulfate. Furthermore, elevated T_{max} (1 to 8 ℃) between No.5 and No.7 was observed, which means the matrix effects within mixed organic compounds can also enhance the T_{max} of organics. The T_{max} of five organic compounds increased by 3 to 17 ℃ with the increase of mass loadings according to No.4 and No.5 (Figure S5). Furthermore, as shown in Figure S6, the T_{max} of five organic compounds generally increases with increased mass loadings, and T_{max} has increased approximately 8 ℃ as the mass loading increases from 200 ng to 1500 ng. The 95% credible intervals of No.5, No.6 and No.7 experiments are significantly larger than the others, which may be attributed to their higher mass loading (1000 ng) than those in other experiments (100 ng, 200 ng and 500 ng) (Figure S7). Therefore, the T_{max} values of organic compounds are affected together by the addition of ammonium sulfate, the matrix effects within organic compounds, and mass loadings. However, these effects cannot be quantified separately in our study. ~~However, mixing ammonium sulfate with five organic compounds together, as done in the fifth (No.5) set of calibration experiments, would increase the T_{max} values of all the five organic standards, among which the T_{max} values of PEGs 6-8 increased by around 20 ˚C. Since there is no obvious difference in T_{max} values between mixed PEGs and stand-alone PEGs, both of which are measured in the absence of ammonium sulfate (Bannan et al., 2019; Ylisirniö et al., 2021), the observed increase in the T_{max} values of five authentic organic standards is likely due to the addition of ammonium sulfate. Ammonium sulfate tends to decrease the volatility of particulate organic compounds, which is likely the cause of the observed matrix effects. A typical example is that the interaction between organic acids and inorganic salts in the particles forms organic salts, which can facilitate the partitioning of organic acids onto the particles (Nie et al., 2017; Yli-Juuti et al., 2013; Zardini et al., 2010). In other words, ammonium sulfate can increase particle viscosity (diffusion limitations within the particles) and interactions of organic and inorganic components within particles (Huang et al., 2018), so that the T_{max} values of authentic organic standards become larger. The extent of this matrix effect may be related to the mass of ammonium sulfate in the particles. The mass of ammonium sulfate was 100 ng in the fourth (No.4) set of calibration experiments whereas this mass was 500 ng in the fifth (No.5) set of experiments. Thus, the T_{max} value, for the same species, measured in the latter case is significantly higher than that measured in the former case. Furthermore, the filter mass loading of the fifth (No.5) set of calibration experiments (1000 ng) was larger than that of the fourth (No.4) set of calibration experiments (200 ng), which may be one of the reasons for the increase in T_{max} value. As there is a synergistic effect between inorganic salts and mass loading, a more detailed study is required.~~

Moreover, the fraction of organic species and inorganic salts of non-refractory submicron aerosol species (NR-PM1) in Beijing in winter 2018 ~~are~~ were about 48% and 52%, respectively (Zhou et al., 2020). The fraction of organic species and inorganic salts ~~of~~ in total particulate matters (PM) in a rural site (Gucheng in Hebei province) in winter 2018 ~~are~~ were about 40% and 60%, respectively (Xu et al., 2021). The mass ratios of the inorganic salt to organic species were close to 1:1 which was similar to that of our laboratory tests (*i.e.,* ~~the fifth (~~No.7~~5)~~ set of calibration experiments). In addition, Ylisirniö et al. (2021) shows that particle size has a moderate impact on the measured T_{max} of organic compounds. The particle size distributions and peak diameters of polydisperse particles in our laboratory experiments (No.4, No.6 and No.7) are similar to those of the ambient samples (Figure S8). Therefore, in our study, particle size distributions have a minor effect on measured T_{max}.

To minimize the uncertainties from multiple factors (e.g., the presence of ammonium sulfate, multiple organic compounds, particle size distributions, and mass loading) on T_{max}, ~~Furthermore, the median mass loading of 30 filter samples collected in our field campaign were around 1100 ng. We thus used~~ the calibration line obtained from No.7 was utilized to estimate T_{max} values of organic compounds in ambient particles and to derive our parameterizations, because the experimental conditions of mimic particle samples in No.7 are the closest to those of the ambient samples and can represent ambient organic aerosol particles.~~by atomizing the mixed solution of ammonium sulfate and five organic standards and collecting 1000 ng particles (the fifth (No.5) set of experiments) to estimate the T_{max} values of organic compounds in ambient particles.~~

3.2 Volatility of OA components

We identified 1,448 compounds from the filter collected on 7:00-7:15, January 15, 2019, in Wangdu, whose mass defect plot is shown in Figure 2. Among them, 340 CHO and 663 CHON species account for ~~a large proportion of~~ 43.5% and 20.8% of the total signals, respectively, because~~owing~~ the ~~to~~ iodide-adduct chemical ionization ~~being~~ is sensitive toward multifunctional oxygenated organic compounds with minimal fragmentation (Bertram et al., 2011; Lopez-Hilfiker et al., 2016). In addition to 326 other species (30.8% of the total signals) that have been assigned with molecular formula~~e~~s but cannot be divided into either the CHO or CHON groups, there are ~~also~~ 119 species (4.9% of the total signals) without attributed molecular formula~~e~~s.

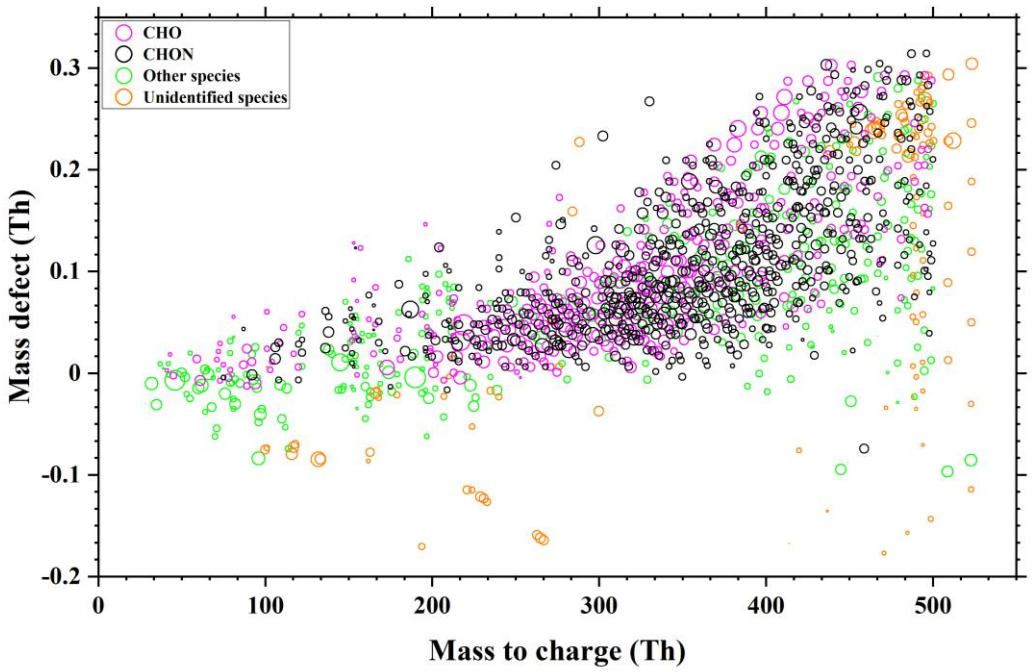

Figure 2. A typical ~~M~~mass defect plot for compounds desorbed from a filter collected on 7:00-7:15, January 15, 2019, in Wangdu. The symbol size is proportional to the logarithm of signal intensity. The reagent ion (I^-) was not removed from their formula~~e~~s.

Among the 1,448 species, we can attribute a T_{max} to 765 species whose thermograms are characterized with a distinguishable T_{max} with one or two desorption peaks, as shown in Figure S~~5~~9a and ~~/S5~~c and Figure S~~5~~9b ~~/~~and ~~S5~~d, and the rest whose thermograms did not show a peak and thus the position of T_{max} cannot be judged, as shown in Figure S~~5~~9e and ~~Figure S5~~f. In Figure S~~6~~10, we show the thermal desorption temperature of these 765 particulate compounds during the FIGAERO-LToF-CIMS analysis. The desorption temperatures of these organic compounds mainly concentrated in the 80~100 ˚C range. The thermograms of most organic compounds show a single peak, and the mass-to-charge ratio (m/z) of these compounds are mainly concentrated in the range of 250~~-~~450 Th, and the dominated compounds are $C_{13}H_{25}NO_2$, $C_{16}H_{32}O_2$, $C_{18}H_{35}NO_4$,

$C_6H_{10}O_5$, $C_9H_{17}NO_2$ and $C_{18}H_{34}O_2$.

We analyzed 30 filter samples in total. For each filter, we selected species that can be assigned~~attributed~~ with a reliable molecular formula in the format of either CHO or CHNO, and species that can be designated with a T_{max}, the intersection of which correspond to species with both reliable CHO/CHNO type molecular formula~~e~~s and T_{max} values. There are 181 such organic compounds including 91 CHO and 90 CHON species that were present in more than 20 out of 30 filter samples. The 181 species are dominant compounds accounting for 34.1% of the total signal of 1448 compounds. It should be noted that several compounds (e.g., $C_3H_8O_3$, CH_2O_2) with high signals in these 1448 compounds were not further analyzed, because they are very volatile at the room temperature (25 ˚C) and their thermograms cannot be characterized with clear T_{max} values from most filter samples.~~–~~ The molecular formula, molecular weight, T_{max}, and C^* calculated according to our calibration in Figure 1 for the 91 CHO and 90 CHON species are summarized in Table S1 and Table S2, respectively.

The thermal behaviors ~~evaporation and decomposition~~ of these 181 organic compounds during the FIGAERO analysis are shown in Figure 3. The cooler ~~-~~peak temperature~~s~~ in ~~a~~ double-peak thermogram~~s~~ mostly appeared in the green rectangular band of 45~80 ˚C, whereas the higher peak ~~temperature~~ temperature~~sone~~ in ~~a~~ double-peak~~s~~ those~~at~~ are~~is~~ mainly the result of thermal decomposition of higher molecular weight organic compounds (Huang et al., 2018), and concentrated in the purple rectangular band of 100~125 ˚C, which is consistent with the result of Wang et al. (2016). On the other hand, the corresponding evaporation temperature for ~~a~~ compound~~s~~ with ~~a~~ single-peak thermogram~~-is~~s ~~–~~concentrated in the red rectangular band of 80~100 ˚C. Clearly, the compounds in Figure 3 can be divided into two groups, as illustrated with the two dashed ellipse~~circle~~s. For each group, the T_{max} values of the single peaks and the cooler ones of ~~a~~ double-peak~~s~~ increase with their corresponding molecular weight, which is consistent with the fact that similar compounds with larger molecular weight tend to possess lower volatility.

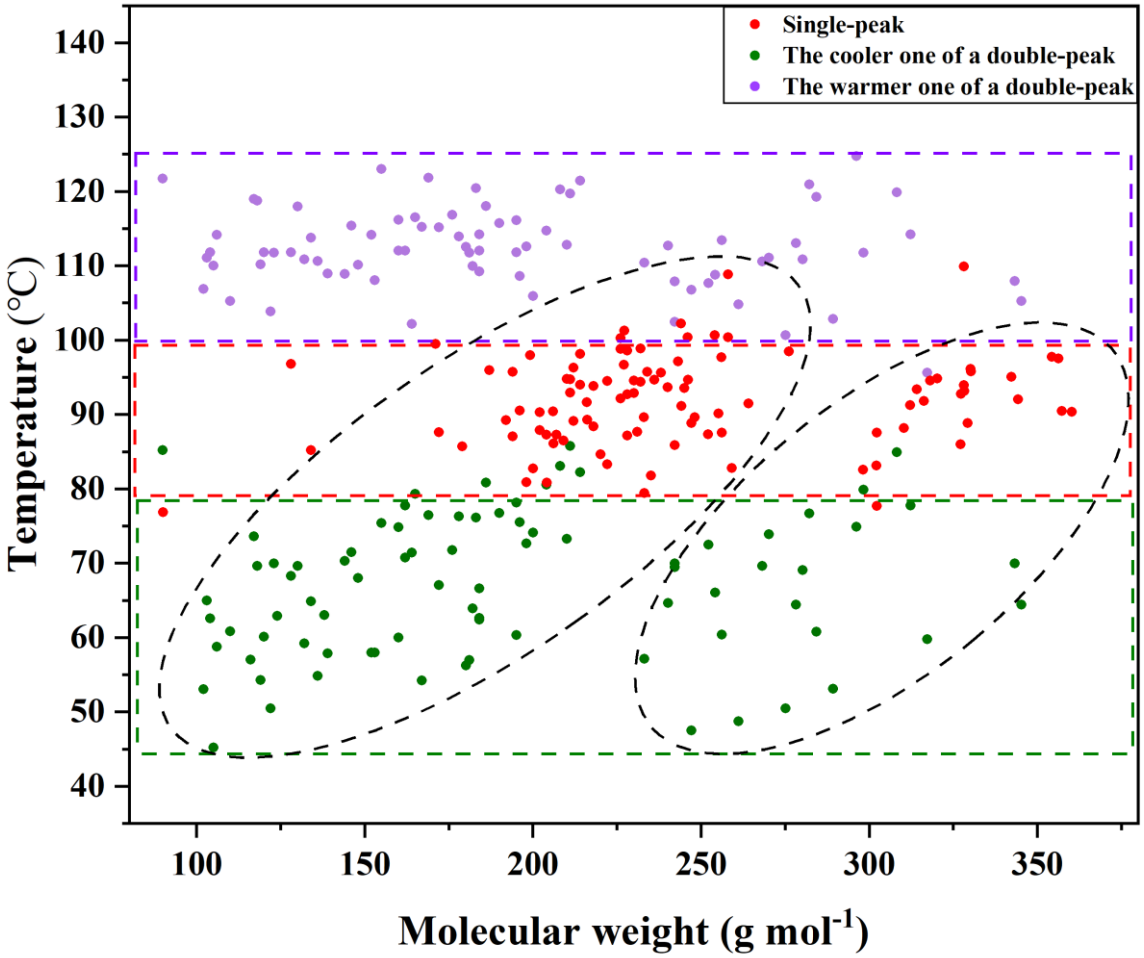

Figure 3. Evaporation and decomposition of 91 CHO and 90 CHON compounds, ~~as illustrated by the temperature of a species' thermogram signal peaks (one or two),~~ of which the reagent ion (I^-) was excluded from their formula~~e~~s. The signal peaks, the cooler and warmer peaks of double-peaks are denoted by red, green and purple circles, respectively. Rectangular bands depict the temperature zones in which peaks appear.

In Figure 4, the T_{max} ~~values~~ of these 181 compounds (91 CHO and 90 CHON) are translated into C^* values according to Eq. (3). Since most of the warmer peaks of double peaks could be from thermal decomposition, t~~T~~he T_{max} ~~data points~~ for the higher-temperature ones in double-peak thermograms of 78 compounds ~~that in fact, do not correspond to a T_{max}~~ are not taken into account~~removed, and the remaining data points are colour scaled with their O/C ratios~~. As shown in Figure 4, the volatilities of CHO and CHON compounds both concentrate in the range of $-4.5 < \log_{10}(C^*) < 1.5$. In addition, CHO and CHON compounds are randomly distributed in two groups according to O/C and there is no obvious distinction~~. It is obvious that these organic compounds can still be divided into two groups.~~ The species in the red dashed ellipse~~circle~~ are the same as those in the left dashed ellipse~~circle~~ in Figure 3, ~~whereas~~ and the compounds in the blue dashed ellipse~~circle~~ are the same as those in the right dashed ellipse~~circle~~. The molecular weights of species in the two groups overlapped, although the ones in the red dashed ellipse~~circle~~ are characterized with relatively lower molecular weights, and the ones in the blue dashed ellipse~~circle~~ are with relatively higher molecular weights. The O/C ratios can clearly distinguish the two groups: 0.56 ± 0.35 (average ± one standard deviation) for the ~~left~~ red ellipse group and 0.18 ± 0.08 for the ~~right~~ blue ellipse group, indicating that the O/C ratio of these compounds could be a key parameter.

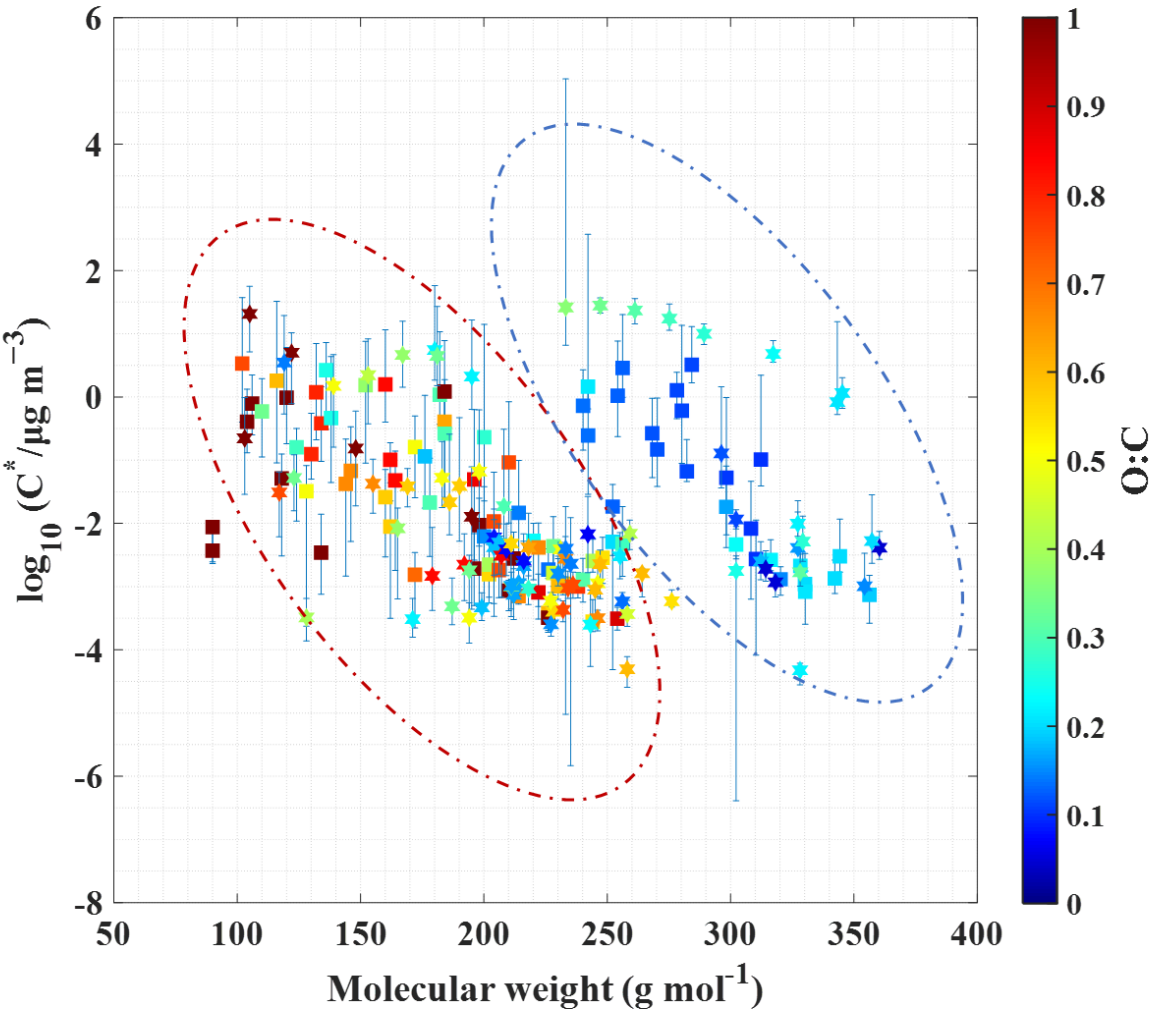
6
4
2
0
-2
-4
-6
-8
50
100
150
200
250
300
350
400
log10 (C*/µg m−3)
Molecular weight (g mol−1)
1
0.9
0.8
0.7
0.6
0.5
0.4
0.3
0.2
0.1
0
O:C

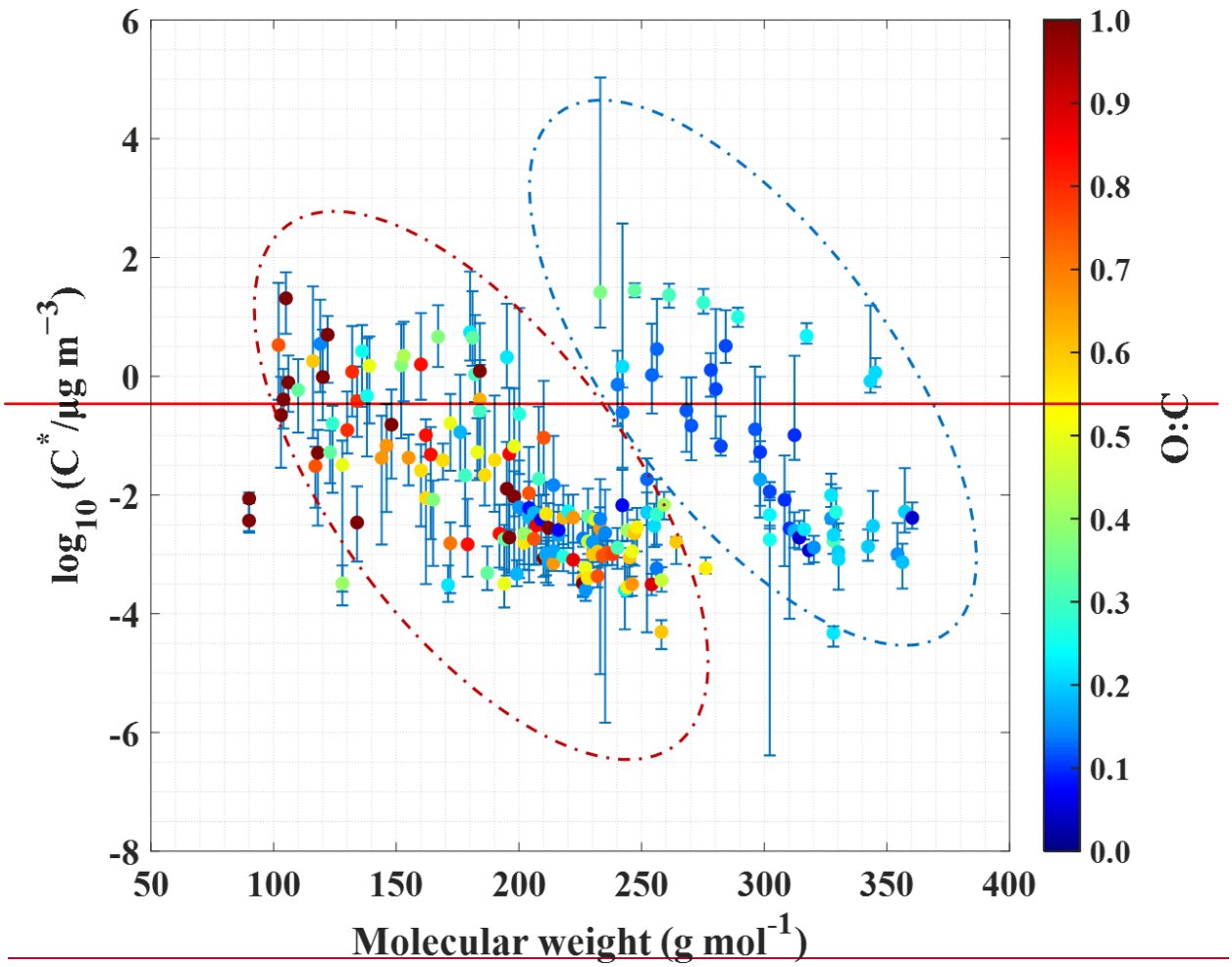

Figure 4. Saturation mass concentration of CHO and CHON compounds against their molecular weights~~molar masses~~, as colour-coded by the ~~molecular~~ O/C ratios. Note that c~~C~~ompounds with an O/C ratio ~~greater than~~ equal to or greater than ~~equal to~~ 1.0 are marked with the same colour. The CHO and CHON compounds are denoted by squares and hexagrams, respectively. Whiskers denote 25th and 75th percentile values of measured saturation mass concentration from ~~total of~~ 30 ambient samples, and whiskers are ultimately due to variability in the measured T_{max} of CHO and CHON compounds. Dashed ellipse~~circle~~s group ~~these~~ compounds on the basis of O/C range.~~with the same key characters.~~

Figure S11~~7~~ clearly shows the O/C characteristics of compounds in the two regions, where the red triangles correspond to those in the red dashed ellipse~~circle~~ of Figure 4, and the blue circles correspond to those in the blue dashed ellipse~~circle~~. The O/C ratios of organic compounds in the red dashed ellipse~~circle~~ ranged from 0.25 to 1.0, and the O/C ratios of those in the blue dashed ellipse~~circle~~ varied between 0-0.25 (Figure S11). ~~The tentative identification of~~ $C_6H_{10}O_5$ (levoglucosan or related isomers) ~~among compounds~~ in the red dashed ellipse~~circle~~, ~~which~~ is a well-accepted tracer of biomass burning OA (BBOA) (Gaston et al., 2016), ~~and of~~ $C_{16}H_{32}O_2$ (palmitic acid), $C_{17}H_{34}O_2$ (margaric acid), $C_{18}H_{32}O_2$ (linoleic acid), and $C_{18}H_{34}O_2$ (oleic acid) ~~among the compounds~~ in the blue dashed ellipse~~circle~~, ~~which~~ have been previously identified as markers of cooking-influenced OA (COA) (Chow et al., 2007; Pei et al., 2016). The correlation coefficients (*Pearson's r*) between $C_6H_{10}O_5$ and 92% of compounds in the red dashed ellipse are from 0.64 to 0.98, and the correlation coefficients between $C_{18}H_{34}O_2$ and 37% of compounds in the blue dashed ellipse are from 0.60 to 0.74.~~The correlation coefficient (Pearson's r) between $C_6H_{10}O_5$ and other compounds in the red dashed circle is 0.88 ± 0.18 (average ± one standard deviation), and the correlation coefficient between $C_{18}H_{34}O_2$ and other compounds in the blue dashed circle is 0.53 ± 0.14.~~ We show examples of the correlation of $C_6H_{10}O_5$, $C_{18}H_{32}O_2$ and other compounds in Figure S12~~8~~. Indeed, there are a number of sources of COA and BBOA near the campaign site, and the campaign was carried out during the heating season. Hence, organic compounds in the red dashed

ellipsecircle may be mainly derived from BBOA, and those in the blue dashed ellipsecircle may be partly derived from COA.

We thus separately optimized the correlation between the molecular elemental composition and the saturation mass concentration of organic compounds in these two regions in Figure 4. As shown in Table 2, the parameterization in of Eq. (4-1) is dedicated for to compounds with O/C ratios of 0.25-1, whereas Eq. (4-2) is more suitable for compounds with O/C ratios of 0-0.25. Mohr et al. (2019) derived parameterization mainly based on HOMs ($-11 < \log_{10}(C^*) < 3$) produced by α-pinene oxidation, whereas Compared with those from Mohr et al. (2019), our fits are mainly based on semi-volatility organic compounds (SVOCs, $10^{-0.5} < C^* \leq 10^{2.5}$) and low-volatility organic compounds (LVOCs, $10^{-4.5} < C^* \leq 10^{-0.5}$), which are predominantly in the particle phase in the atmosphere.

Table 2. The volatility parameterizations of this study and cited literature. In this study, tThe improved parameterizations of saturation mass concentration were modified by the least-square optimization from Eq. (4). The best-fit parameters were obtained at 298 K. Where the parameter n_c^0 = 25, it is the baseline carbon backbone for the volatility of 1 $\mu g\ m^{-3}$ without adding any functional groups (Donahue et al., 2011; Stolzenburg et al., 2018).

	n_c^0	b_c	b_o	b_{co}	b_N	Suggested O/C range	b_{add}
Eq. (4-1) in this study	25	0.0700	0.6307	-0.0615	2.3962	0.25-1	/
Eq. (4-2) in this study	25	0.2075	2.8276	-1.0744	1.8223	0-0.25	/
Donahue et al. (2011)	25	0.475	2.3	-0.3	/	/	/
Mohr et al. (2019)	25	0.475	0.2	0.9	2.5	/	/
Stolzenburg et al. (2018) (monomers)	25	0.475	2.3	-0.3	/	/	0.90
Stolzenburg et al. (2018) (dimers)	25	0.475	2.3	-0.3	/	/	1.13
Li et al. (2016) (CHO)	22.66	0.4481	1.656	-0.7790	/	/	/
Li et al. (2016) (CHON)	24.13	0.3667	0.7732	-0.07790	1.114	/	/

4 Atmospheric implications

For ambient studies, it is crucial to develop a more accurate empirical formula to estimate the volatility of organics in particles. Parametrization in Donahue et al. (2011) is mainly based on mono-functional compounds such as alcohol, aldehyde, acid and etc., and could cause a large uncertainty when estimating the volatility of compounds in the range $-5 < \log_{10}(C^*) < 2$ and $1{:}3 < O/C < 1{:}1$, because volatilities in this region are extrapolated with volatilities of compounds with simpler molecular formulaes (Donahue et al., 2011). In addition, compounds in this region may be characterized with multiple functionalities, which are also lacking as reference standards in the Donahue et al. (2011) study. Compounds in this region can be roughly regarded as oxygenated organic aerosols (OOAs) (Donahue et al., 2011). In our study, a yellow dashed frame is used to mark this region in Figure S117, which is occupied by organic compounds that are concentrated in the red dashed ellipsecircle of Figure 4. Furthermore, we used the 15 highly oxygenated organic molecules (HOMs) with O/C ratios of 0.25-1 whose volatility was estimated by the SIMPOL method (Pankow and Asher, 2008) in the Tröstl et al., (2016) study and 230 CHO compounds with O/C ratios of 0.25-1 as benchmarks to compare the performance of different parameterization methods, as shown in Figure 5(a). The volatilities of 15 HOMs was obtained by SIMPOL from the Tröstl et al. (2016) study. The 230 CHO (O/C: 0.25-1) compounds are from Zhao et al. (2013) and Mazzoleni et al. (2010), because predicted molecular structures of these 230 compounds are reliable. As expected, volatilities predicted by the Donahue et al. (2011) parameterization are not consistent with those by the SIMPOL method. Although Mohr et al. (2019) updated parametrization based on those 15 HOMs detected by Tröstl et al., (2016), the volatility predicted by the Mohr et al. (2019) parameterization does not match those by the SIMPOL method very well, which could be explained by not considering covalent binding, using the same parameterization for dimer and monomer may cause deviations. On the other hand, the accuracy in predication of volatility accuracy of the parameterizations of Stolzenburg et al. (2018), Li et al. (2016), and Eq. (4-1) is generally comparable (Figure 5a), although a

~~few data points are more off from the 1:1 line~~. Compared to the parameterizations of Stolzenburg et al. (2018) and Li et al. (2016), the consistency between the parameterization of Eq. (4-1) and SIMPOL is not as good for the more volatile compounds ($\log_{10}(C^*) > 0.5$), but the consistency is better for the LVOCs ($10^{-4.5} < C^* \leq 10^{-0.5}$), which reflects the inherent strength and deficiency of the FIGAERO method. One of reasons may be that in this study, we used the saturation mass concentration (C^*) of five organic standards concentrates in the range of $-5 < \log_{10}(C^*) < 0.5$, as shown in Figure S13. Moreover, the parameterization of Eq. (4-1) was derived based on the ambient compounds in the red dashed ellipse of Figure 4, whose volatilities predominantly concentrate in the range of $-4.5 < \log_{10}(C^*) < 1.5$. ~~Stolzenburg et al. (2018) modified parameterization also based on those 15 HOMs and fitted dimer and monomer separately, allowing their parameters to include the covalent binding. Li et al. (2016) developed parameterization based on 31066 compounds from the NCI open database, which contain 8420 CHO compounds with O/C ratios ranging from 0 to 1. Therefore, the parameterizations of Stolzenburg et al. (2018) and Li et al. (2016) agree well with that of the SIMPOL method. The parameterization of Eq. (4-1) based on the compounds in the red dashed circle of Figure 4 contain lots of OOAs species (e.g., 32 HOMs). Thus the Eq. (4-1) can accurately estimate the volatility of ambient OOAs.~~

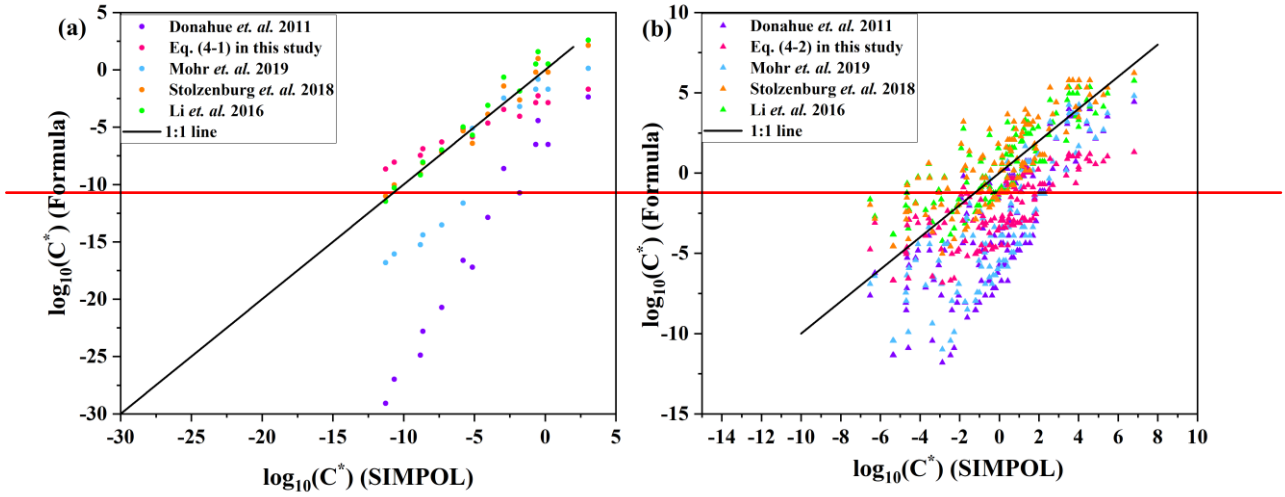

~~Figure 5. (a) Saturation mass concentration (C^*) of 15 HOMs (O/C:0.25-1) estimated by Eq. (4-1) in this study, and parametrizations from Donahue et al. (2011), Mohr rt al. (2019), Stolzenburg et al. (2018), and Li et al. (2016), respectively, against that estimated by the SIMPOL method. (b) Saturation mass concentration (C^*) of 132 CHO compounds (O/C:0-0.25) estimated by Eq. (4-2) in this study, and parametrizations from Donahue et al. (2011), Mohr et al. (2019), Stolzenburg et al. (2018), and Li et al. (2016), respectively, against that estimated by the SIMPOL method.~~

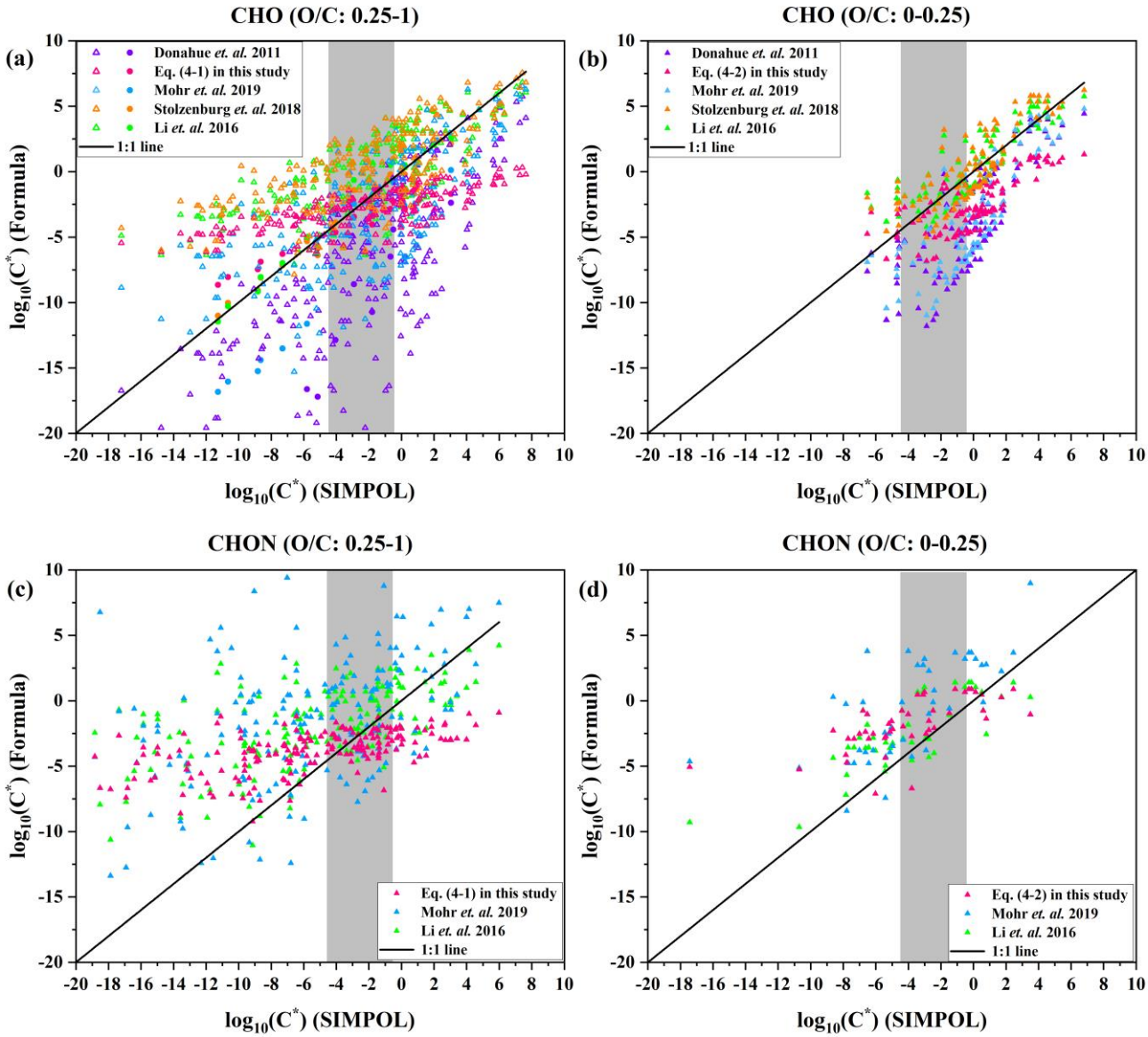

Figure 5. Saturation mass concentration (C^*) of 15 HOMs (O/C: 0.25-1) and 230 CHO compounds (O/C: 0.25-1) estimated by Eq. (4-1) **(a)**, 106 CHO compounds (O/C: 0-0.25) estimated by Eq. (4-2) **(b)**, 183 CHON compounds (O/C: 0.25-1) estimated by Eq. (4-1) **(c)**, 46 CHON compounds (O/C: 0-0.25) estimated by Eq. (4-2) **(d)** and the parametrizations from Donahue et al. (2011), Mohr et al. (2019), Stolzenburg et al. (2018), and Li et al. (2016), against that estimated by SIMPOL. In panel a, the 15 HOMs are denoted by circles and 230 CHO compounds are denoted by triangles. The 230 CHO (O/C: 0.25-1), 106 CHO (O/C: 0-0.25), 183 CHON (O/C: 0.25-1) and 46 CHON (O/C: 0-0.25) compounds are from Zhao et al. (2013) and Mazzoleni et al. (2010) field campaigns. The grey colored band denotes low-volatility organic compounds (LVOCs).

Also, w~~W~~e ~~also~~ selected 10~~632~~ CHO compounds with O/C ratios of 0-0.25 ~~as~~ from compounds observed ~~either in this study or from~~ by ~~the~~ Zhao et al. (2013) and Mazzoleni et al. (2010) ~~field campaigns.~~, The ~~whose~~ saturation mass concentration (C^*) of these compounds are estimated by different parameterizations and ~~the~~ SIMPOL ~~method~~. ~~Common structures and functional groups were selected to calculate the volatility of 132 organic compounds by the SIMPOL method.~~ As shown in Figure 5(~~b~~), volatilities predicted by the Donahue et al. (2011) parameterization is ~~quite~~ off those by ~~the~~ SIMPOL ~~method~~, this is mainly because the parameterization was developed according to higher volatility of organic compounds whose volatilities concentrate~~d~~ in the range of $0 < \log_{10}(C^*) < 9$, but those selected ~~132~~ 106 CHO compounds with lower volatility whose volatilities concentrate in the range of $-6 < \log_{10}(C^*) < 6$. Although Mohr et al. (2019) updated parametrization based on ~~those~~ 15 HOMs whose volatilities concentrate in the range of $-11 < \log_{10}(C^*) < 3$, volatilities predicted by Mohr et al.

(2019) parameterization still is ~~quite~~ off those by ~~the~~ SIMPOL ~~method~~. This is mainly because those ~~132~~ 106 CHO compounds with lower O/C (0-0.25), but the O/C of those 15 HOMs is 0.25-1. Compared to the parameterizations of Stolzenburg et al. (2018) and Li et al. (2016), in general, the Eq. (4-2) parameterization does not match SIMPOL as well. However, the parameterizations of Stolzenburg et al. (2018), Li et al. (2016) and Eq. (4-2) are comparable for LVOCs. This may be again explained by the difference between the C^* of our organic standards in the literature and those calculated by SIMPOL and by the volatility distribution of organic standards (Figure S13)~~-~~.

We selected 183 CHON compounds with O/C ratios of 0.25-1 and 46 CHON compounds with O/C ratios of 0-0.25 from Zhao et al. (2013) and Mazzoleni et al. (2010). The molecular structures of selected species can be reliably predicted, and then their saturation mass concentration (C^*) are estimated by different parameterizations and SIMPOL, respectively. The parameterizations of Donahue et al. (2011) and Stolzenburg et al. (2018) relies only on carbon and oxygen number and do not explicitly mention the nitrogen coefficient (b_N), thus these two parameterizations are excluded from the comparison of the volatility of CHON compounds. As shown in Figure 5c, the performance of Eq. (4-1) parameterization for CHON compounds (O/C: 0.25-1) is similar to that for CHO compounds (O/C: 0.25-1) (Figure 5a). The volatilities LVOCs predicted by the Eq. (4-1) parameterization are more consistent with SIMPOL than the parameterizations of Li et al. (2016). In Figure 5d, the volatilities of CHON compounds (O/C: 0-0.25) predicted by the parameterizations of Li et al. (2016) and our study are comparable, and most of the data points are close to the 1:1 line. The volatility of CHON compounds predicted by the Mohr et al. (2019) parameterization does not match those by SIMPOL very well.

~~Furthermore, we selected 42 alcohols, aldehydes, acids and diols with O/C ratios of 0–0.25 from NIST, whose saturation mass concentration C^* are estimated by different parameterizations. As shown in Figure S9, the volatilities predicted by the Donahue et al. (2011), Mohr et al. (2019), Stolzenburg et al. (2018) and the Li et al. (2016) parameterizations agree well with values in NIST, showing better agreement than the Eq. (4-2) parameterizations. The reason is that we modified parameterizations based on SVOCs ($10^{-0.5} < C^* \leq 10^{2.5}$) and LVOCs ($10^{-4.5} < C^* \leq 10^{-0.5}$), but these 42 compounds predominantly concentrate in the range of intermediate volatility organic compounds (IVOCs, $10^{2.5} < C^*$) (Schervish and Donahue, 2020).~~

Although the applicability of ~~Li et al. (2016) and Stolzenburg et al. (2018)~~ the ~~developed~~ parameterizations of Li et al. (2016) and Stolzenburg et al. (2018) is more extensive and ~~can accurately estimate~~ the volatilities~~y of single IVOCs, SVOCs, LVOCs and extremely low volatility organic compounds (ELVOCs, $C^* \leq 10^{-4.5}$)~~ estimated by these two parameterizations agree well with SIMPOL, Li et al. (2016) and Stolzenburg et al. (2018) modified parameterizations based on a large number of organic species from NCI open database and SIMPOL calculations, respectively. However, the parameterizations of Eq. (4-1) and Eq. (4-2) were derived from organic compounds with different O/C ratios in ambient particles, whose volatilities were estimated by the calibration experiments instead of SIMPOL. Therefore, Eq. (4-1) and Eq. (4-2) can better represent the volatility of ambient organic aerosols. In addition, in Figure 5, for LVOCs, the volatility estimation by Eq. (4-1) and Eq. (4-2) is better than Li et al. (2016) and Stolzenburg et al. (2018). Compared with the ELVOCs, IVOCs and SVOCs, the LVOCs have a dominant contribution to particle growth in new particle formation events. Hence, our parameterizations could be well applied to assess the condensational growth of newly formed particles.~~, the Li et al. (2016) parameterization are statistical results based on the NCI open database, and a large number of organic species are needed. Stolzenburg et al. (2018) parameterization added a free parameter b_{add} that included the covalent binding and yielded different values for monomers and dimers. Compared with previous volatility parameterizations, the improved Eq. (4-1) and Eq. (4-2) in this study can better estimate the volatility of SVOCs and LVOCs in the ambient organic aerosols. The volatility estimated by the Eq. (4-2) parameterization is lower than that estimated by the Li et al. (2016) and Stolzenburg et al. (2018) parameterizations, this may be because the matrix effect of inorganic salts has a more obvious effect on organic compounds with large molecular weights, which is supported by the result of calibration experiments that the increase in the T_{max} of PEG-6 (molecular weight: 282.33 Da), PEG-7 (molecular weight: 326.39 Da) and PEG-8 (molecular weight: 370.44 Da) is greater than that of erythritol (molecular weight: 122.12 Da) and citric acid (molecular weight: 192.12 Da) in the fifth (No.5) set of calibration experiments, as shown in Figure S4. And the Eq. (4-2) parameterization are developed based on organic compounds with large molecular

~~weights in the blue dashed circle of Figure 4. Therefore, it is reasonable that there is a certain discrepancy between the volatility estimated by the improved Eq. (4-1) and Eq. (4-2) based on organic compounds in ambient particles and estimated by the modified parameterizations of Li et al. (2016) and Stolzenburg et al. (2018) based on single and several mixed organic compounds.~~

In summary, our study developed empirical volatility-molecular formula functions (Eq. (4-1) and ~~the~~ Eq. (4-2)), based on measured C^* of selected CHO and CHON compounds in ambient particles. The parameterizations of Eq. (4-1) and Eq. (4-2) can more accurately predict~~more accurately predict~~ the volatility of ~~SVOCs and~~ LVOCs with higher O/C (0.25-1) and lower O/C (0-0.25) in the ambient organic aerosols, respectively, owning to the nature of the FIGAERO method. ~~The Eq. (4-2) can more accurately predict the volatility of SVOCs and LVOCs with lower O/C (0-0.25) in the ambient organic aerosols.~~ The comparison with previous empirical functions suggests that it is feasible to modify empirical functions based on atmospheric organic compounds with unknown structures and functional groups using calibration experiments. When analyzing the volatility of atmospheric organic aerosols, it is suggested~~ more reasonable and scientific~~ to~~ add inorganic salts to organic standards and use the atomization method to~~ create the calibration curve from experiments with the same conditions as that of ambient samples, because the addition of inorganic salts~~ account~~, mixing of organic compounds, mass loadings, and particle size distributions could together ~~ for around half of atmospheric organic aerosols particles and the~~ influence T_{max} values of organic compounds~~effect of inorganic salts is not negligible~~. ~~Compared with the syringe deposition method, the atomization method shows much better repeatability.~~ Furthermore, we suggest there should be specialized volatility parameterization for different O/C compounds.

Data availability. More detailed data can be provided by contacting the corresponding authors.

Author contributions. LW designed the study. GY, YLL and YQL conducted the field campaign. SR, YW, YYL, LHW, GY and YLL carried out laboratory experiments. SR analyzed the data. SR, LW and LY wrote the paper with contributions from all of the other co-authors.

Competing interest. The authors declare that they have no conflicts of interest.

Acknowledgement. This research has been supported by the National Natural Science Foundation of China (21925601 and 92044301).

References

Bannan, T. J., Le Breton, M., Priestley, M., Worrall, S. D., Bacak, A., Marsden, N. A., Mehra, A., Hammes, J., Hallquist, M., Alfarra, M. R., Krieger, U. K., Reid, J. P., Jayne, J., Robinson, W., McFiggans, G., Coe, H., Percival, C. J. and Topping, D.: A method for extracting calibrated volatility information from the FIGAERO-HR-ToF-CIMS and its experimental application, Atmos. Meas. Tech., 12(3), 1429–1439, doi:10.5194/amt-12-1429-2019, 2019.

Bertram, T. H., Kimmel, J. R., Crisp, T. A., Ryder, O. S., Yatavelli, R. L. N., Thornton, J. A., Cubison, M. J., Gonin, M. and Worsnop, D. R.: A field-deployable, chemical ionization time-of-flight mass spectrometer, Atmos. Meas. Tech., 4(7), 1471–1479, doi:10.5194/amt-4-1471-2011, 2011.

Capouet, M. and Müller, J.-F.: A group contribution method for estimating the vapour pressures of α-pinene oxidation products, Atmos. Chem. Phys., 6(6), 1455–1467, doi:10.5194/acp-6-1455-2006, 2006.

Chow, J. C., Watson, J. G., Lowenthal, D. H., Chen, L. W. A., Zielinska, B., Mazzoleni, L. R. and Magliano, K. L.: Evaluation of organic markers for chemical mass balance source apportionment at the Fresno Supersite, Atmos. Chem. Phys., 7(7), 1741–1754, doi:10.5194/acp-7-1741-2007, 2007.

Donahue, N. M., Robinson, A. L. and Pandis, S. N.: Atmospheric organic particulate matter: From smoke to secondary organic aerosol, Atmos. Environ., 43(1), 94–106, doi:10.1016/j.atmosenv.2008.09.055, 2009.

Donahue, N. M., Epstein, S. A., Pandis, S. N. and Robinson, A. L.: A two-dimensional volatility basis set: 1. organic-aerosol mixing thermodynamics, Atmos. Chem. Phys., 11(7), 3303–3318, doi:10.5194/acp-11-3303-2011, 2011.

Drisdell, W. S., Saykally, R. J. and Cohen, R. C.: On the evaporation of ammonium sulfate solution, Proc. Natl. Acad. Sci. U. S. A., 106(45), 18897–18901, doi:10.1073/pnas.0907988106, 2009.

Eichler, P., Müller, M., D'Anna, B. and Wisthaler, A.: A novel inlet system for online chemical analysis of semi-volatile submicron particulate matter, Atmos. Meas. Tech., 8(3), 1353–1360, doi:10.5194/amt-8-1353-2015, 2015.

Faulhaber, A. E., Thomas, B. M., Jimenez, J. L., Jayne, J. T., Worsnop, D. R. and Ziemann, P. J.: Characterization of a thermodenuder-particle beam mass spectrometer system for the study of organic aerosol volatility and composition, Atmos. Meas. Tech., 2(1), 15–31, doi:10.5194/amt-2-15-2009, 2009.

Gaston, C. J., Lopez-Hilfiker, F. D., Whybrew, L. E., Hadley, O., McNair, F., Gao, H., Jaffe, D. A. and Thornton, J. A.: Online molecular characterization of fine particulate matter in Port Angeles, WA: Evidence for a major impact from residential wood smoke, Atmos. Environ., 138, 99–107, doi:10.1016/j.atmosenv.2016.05.013, 2016.

Goodman, K. J. and Brenna, J. T.: Curve Fitting for Restoration of Accuracy for Overlapping Peaks in Gas Chromatography/Combustion Isotope Ratio Mass Spectrometry, Anal. Chem., 66(8), 1294–1301, doi:10.1021/ac00080a015, 1994.

Huang, W., Saathoff, H., Pajunoja, A., Shen, X., Naumann, K. H., Wagner, R., Virtanen, A., Leisner, T. and Mohr, C.: α-Pinene secondary organic aerosol at low temperature: Chemical composition and implications for particle viscosity, Atmos. Chem. Phys., 18(4), 2883–2898, doi:10.5194/acp-18-2883-2018, 2018.

Huang, W., Saathoff, H., Shen, X., Ramisetty, R., Leisner, T. and Mohr, C.: Seasonal characteristics of organic aerosol chemical composition and volatility in Stuttgart, Germany, Atmos. Chem. Phys., 19(18), 11687–11700, doi:10.5194/acp-19-11687-2019, 2019.

Isaacman-Vanwertz, G. and Aumont, B.: Impact of organic molecular structure on the estimation of atmospherically relevant physicochemical parameters, Atmos. Chem. Phys., 21(8), 6541–6563, doi:10.5194/acp-21-6541-2021, 2021.

Jimenez, J. L., Canagaratna, M. R., Donahue, N. M., Prevot, A. S. H., Zhang, Q., Kroll, J. H., DeCarlo, P. F., Allan, J. D., Coe, H., Ng, N. L., Aiken, A. C., Docherty, K. S., Ulbrich, I. M., Grieshop, A. P., Robinson, A. L., Duplissy, J., Smith, J. D., Wilson, K. R., Lanz, V. A., Hueglin, C., Sun, Y. L., Tian, J., Laaksonen, A., Raatikainen, T., Rautiainen, J., Vaattovaara, P., Ehn, M., Kulmala, M., Tomlinson, J. M., Collins, D. R., Cubison, M. J., Dunlea, E. J., Huffman, J. A., Onasch, T. B., Alfarra, M. R., Williams, P. I., Bower, K., Kondo, Y., Schneider, J., Drewnick, F., Borrmann, S., Weimer, S., Demerjian, K., Salcedo, D., Cottrell, L., Griffin, R., Takami, A., Miyoshi, T., Hatakeyama, S., Shimono, A., Sun, J. Y., Zhang, Y. M., Dzepina, K., Kimmel, J. R., Sueper, D., Jayne, J. T., Herndon, S. C., Trimborn, A. M., Williams, L. R., Wood, E. C., Middlebrook, A. M., Kolb, C. E., Baltensperger, U. and Worsnop, D. R.: Evolution of organic aerosols in the atmosphere, Science (80-.)., 326(5959), 1525–1529, doi:10.1126/science.1180353, 2009.

Lee, B. H., Lopez-Hilfiker, F. D., Mohr, C., Kurtén, T., Worsnop, D. R. and Thornton, J. A.: An iodide-adduct high-resolution time-of-flight chemical-ionization mass spectrometer: Application to atmospheric inorganic and organic compounds, Environ. Sci. Technol., 48(11), 6309–6317, doi:10.1021/es500362a, 2014.

Li, H., Zhang, Q., Zhang, Q., Chen, C., Wang, L., Wei, Z., Zhou, S., Parworth, C., Zheng, B., Canonaco, F., Prévôt, A. S. H., Chen, P., Zhang, H., Wallington, T. J. and He, K.: Wintertime aerosol chemistry and haze evolution in an extremely polluted city of the North China Plain: Significant contribution from coal and biomass combustion, Atmos. Chem. Phys., 17(7), 4751–4768, doi:10.5194/acp-17-4751-2017, 2017.

Li, Y., Pöschl, U. and Shiraiwa, M.: Molecular corridors and parameterizations of volatility in the chemical evolution of organic aerosols, Atmos. Chem. Phys., 16(5), 3327–3344, doi:10.5194/acp-16-3327-2016, 2016.

Lopez-Hilfiker, F. D., Mohr, C., Ehn, M., Rubach, F., Kleist, E., Wildt, J., Mentel, T. F., Lutz, A., Hallquist, M., Worsnop, D. and Thornton, J. A.: A novel method for online analysis of gas and particle composition: Description and evaluation of a filter inlet for gases and AEROsols (FIGAERO), Atmos. Meas. Tech., 7(4), 983–1001, doi:10.5194/amt-7-983-2014, 2014.

Lopez-Hilfiker, F. D., Mohr, C., Ehn, M., Rubach, F., Kleist, E., Wildt, J., Mentel, T. F., Carrasquillo, A. J., Daumit, K. E., Hunter, J. F., Kroll, J. H., Worsnop, D. R. and Thornton, J. A.: Phase partitioning and volatility of secondary organic aerosol components formed from α-pinene ozonolysis and OH oxidation: The importance of accretion products and other low volatility compounds, Atmos. Chem. Phys., 15(14), 7765–7776, doi:10.5194/acp-15-7765-2015, 2015.

Lopez-Hilfiker, F. D., Mohr, C., D'Ambro, E. L., Lutz, A., Riedel, T. P., Gaston, C. J., Iyer, S., Zhang, Z., Gold, A., Surratt, J. D., Lee, B. H., Kurten, T., Hu, W. W., Jimenez, J., Hallquist, M. and Thornton, J. A.: Molecular Composition and Volatility of Organic Aerosol in the Southeastern U.S.: Implications for IEPOX Derived SOA, Environ. Sci. Technol., 50(5), 2200–2209, doi:10.1021/acs.est.5b04769, 2016.

Mazzoleni, L. R., Ehrmann, B. M., Shen, X., Marshall, A. G. and Collett, J. L.: Water-Soluble Atmospheric Organic Matter in Fog: Exact Masses and Chemical Formula Identification by Ultrahigh-Resolution Fourier Transform Ion Cyclotron Resonance Mass Spectrometry, Environ. Sci. Technol., 44(10), 3690–3697, doi:10.1021/es903409k, 2010.

Mohr, C., Thornton, J. A., Heitto, A., Lopez-Hilfiker, F. D., Lutz, A., Riipinen, I., Hong, J., Donahue, N. M., Hallquist, M., Petäjä, T., Kulmala, M. and Yli-Juuti, T.: Molecular identification of organic vapors driving atmospheric nanoparticle growth, Nat. Commun., 10(1), 1–7, doi:10.1038/s41467-019-12473-2, 2019.

Nah, T., Xu, L., Osborne-Benthaus, K. A., White, S. M., France, S. and Ng, N. L.: Mixing order of sulfate aerosols and isoprene epoxydiols affects secondary organic aerosol formation in chamber experiments, Atmos. Environ., 217(September), 116953, doi:10.1016/j.atmosenv.2019.116953, 2019.

Pankow, J. F. and Asher, W. E.: SIMPOL.1: A simple group contribution method for predicting vapor pressures and enthalpies of vaporization of multifunctional organic compounds, Atmos. Chem. Phys., 8(10), 2773–2796, doi:10.5194/acp-8-2773-2008, 2008.

Pei, B., Cui, H., Liu, H. and Yan, N.: Chemical characteristics of fine particulate matter emitted from commercial cooking, Front. Environ. Sci. Eng., 10(3), 559–568, doi:10.1007/s11783-016-0829-y, 2016.

Shiraiwa, M. and Seinfeld, J. H.: Equilibration timescale of atmospheric secondary organic aerosol partitioning, Geophys. Res. Lett., 39(24), 2012GL054008, doi:10.1029/2012GL054008, 2012.

Smith, J. N., Moore, K. F., McMurry, P. H. and Eisele, F. L.: Atmospheric Measurements of Sub-20 nm Diameter Particle Chemical Composition by Thermal Desorption Chemical Ionization Mass Spectrometry, Aerosol Sci. Technol., 38(2), 100–110, doi:10.1080/02786820490249036, 2004.

Stark, H., Yatavelli, R. L. N., Thompson, S. L., Kang, H., Krechmer, J. E., Kimmel, J. R., Palm, B. B., Hu, W., Hayes, P. L., Day, D. A., Campuzano-Jost, P., Canagaratna, M. R., Jayne, J. T., Worsnop, D. R. and Jimenez, J. L.: Impact of Thermal Decomposition on Thermal Desorption Instruments: Advantage of Thermogram Analysis for Quantifying Volatility Distributions of Organic Species, Environ. Sci. Technol., 51(15), 8491–8500, doi:10.1021/acs.est.7b00160, 2017.

Stocker, T. F., D. Qin, G.-K., Plattner, M. T., Allen, S. K., Boschung, J., Nauels, A., Xia, Y., Bex, V. and Midgley, P. M.: IPCC, 2013: Summary for Policymakers. In: Climate Change 2013: The Physical Science Basis. Contribution of Working Group I to the Fifth Assessment Report of the IPCC., 2013.

Stolzenburg, D., Fischer, L., Vogel, A. L., Heinritzi, M., Schervish, M., Simon, M., Wagner, A. C., Dada, L., Ahonen, L. R.,

Amorim, A., Baccarini, A., Bauer, P. S., Baumgartner, B., Bergen, A., Bianchi, F., Breitenlechner, M., Brilke, S., Mazon, S. B., Chen, D., Dias, A., Draper, D. C., Duplissy, J., Haddad, I. El, Finkenzeller, H., Frege, C., Fuchs, C., Garmash, O., Gordon, H., He, X., Helm, J., Hofbauer, V., Hoyle, C. R., Kim, C., Kirkby, J., Kontkanen, J., Kürten, A., Lampilahti, J., Lawler, M., Lehtipalo, K., Leiminger, M., Mai, H., Mathot, S., Mentler, B., Molteni, U., Nie, W., Nieminen, T., Nowak, J. B., Ojdanic, A., Onnela, A., Passananti, M., Petäjä, T., Quéléver, L. L. J., Rissanen, M. P., Sarnela, N., Schallhart, S., Tauber, C., Tomé, A., Wagner, R., Wang, M., Weitz, L., Wimmer, D., Xiao, M., Yan, C., Ye, P., Zha, Q., Baltensperger, U., Curtius, J., Dommen, J., Flagan, R. C., Kulmala, M., Smith, J. N., Worsnop, D. R., Hansel, A., Donahue, N. M. and Winkler, P. M.: Rapid growth of organic aerosol nanoparticles over a wide tropospheric temperature range, Proc. Natl. Acad. Sci. U. S. A., 115(37), 9122–9127, doi:10.1073/pnas.1807604115, 2018.

Thornton, J. A., Mohr, C., Schobesberger, S., D'Ambro, E. L., Lee, B. H. and Lopez-Hilfiker, F. D.: Evaluating Organic Aerosol Sources and Evolution with a Combined Molecular Composition and Volatility Framework Using the Filter Inlet for Gases and Aerosols (FIGAERO), Acc. Chem. Res., 53(8), 1415–1426, doi:10.1021/acs.accounts.0c00259, 2020.

Tröstl, J., Chuang, W. K., Gordon, H., Heinritzi, M., Yan, C., Molteni, U., Ahlm, L., Frege, C., Bianchi, F., Wagner, R., Simon, M., Lehtipalo, K., Williamson, C., Craven, J. S., Duplissy, J., Adamov, A., Almeida, J., Bernhammer, A. K., Breitenlechner, M., Brilke, S., Dias, A., Ehrhart, S., Flagan, R. C., Franchin, A., Fuchs, C., Guida, R., Gysel, M., Hansel, A., Hoyle, C. R., Jokinen, T., Junninen, H., Kangasluoma, J., Keskinen, H., Kim, J., Krapf, M., Kürten, A., Laaksonen, A., Lawler, M., Leiminger, M., Mathot, S., Möhler, O., Nieminen, T., Onnela, A., Petäjä, T., Piel, F. M., Miettinen, P., Rissanen, M. P., Rondo, L., Sarnela, N., Schobesberger, S., Sengupta, K., Sipilä, M., Smith, J. N., Steiner, G., Tomè, A., Virtanen, A., Wagner, A. C., Weingartner, E., Wimmer, D., Winkler, P. M., Ye, P., Carslaw, K. S., Curtius, J., Dommen, J., Kirkby, J., Kulmala, M., Riipinen, I., Worsnop, D. R., Donahue, N. M. and Baltensperger, U.: The role of low-volatility organic compounds in initial particle growth in the atmosphere, Nature, 533(7604), 527–531, doi:10.1038/nature18271, 2016.

Wang, D. S. and Hildebrandt Ruiz, L.: Chlorine-initiated oxidation of alkanes under high-NO conditions: Insights into secondary organic aerosol composition and volatility using a FIGAERO-CIMS, Atmos. Chem. Phys., 18(21), 15535–15553, doi:10.5194/acp-18-15535-2018, 2018.

Wang, M., Yao, L., Zheng, J., Wang, X., Chen, J., Yang, X., Worsnop, D. R., Donahue, N. M. and Wang, L.: Reactions of Atmospheric Particulate Stabilized Criegee Intermediates Lead to High-Molecular-Weight Aerosol Components, Environ. Sci. Technol., 50(11), 5702–5710, doi:10.1021/acs.est.6b02114, 2016.

Wang, M., Chen, D., Xiao, M., Ye, Q., Stolzenburg, D., Hofbauer, V., Ye, P., Vogel, A. L., Mauldin, R. L., Amorim, A., Baccarini, A., Baumgartner, B., Brilke, S., Dada, L., Dias, A., Duplissy, J., Finkenzeller, H., Garmash, O., He, X. C., Hoyle, C. R., Kim, C., Kvashnin, A., Lehtipalo, K., Fischer, L., Molteni, U., Petäjä, T., Pospisilova, V., Quéléver, L. L. J., Rissanen, M., Simon, M., Tauber, C., Tomé, A., Wagner, A. C., Weitz, L., Volkamer, R., Winkler, P. M., Kirkby, J., Worsnop, D. R., Kulmala, M., Baltensperger, U., Dommen, J., El-Haddad, I. and Donahue, N. M.: Photo-oxidation of Aromatic Hydrocarbons Produces Low-Volatility Organic Compounds, Environ. Sci. Technol., 54(13), 7911–7921, doi:10.1021/acs.est.0c02100, 2020a.

Wang, Y., Mehra, A., Krechmer, J. E., Yang, G., Hu, X., Lu, Y., Lambe, A., Canagaratna, M., Chen, J., Worsnop, D., Coe, H. and Wang, L.: Oxygenated products formed from OH-initiated reactions of trimethylbenzene: Autoxidation and accretion, Atmos. Chem. Phys., 20(15), 9563–9579, doi:10.5194/acp-20-9563-2020, 2020b.

Xu, W., Chen, C., Qiu, Y., Li, Y., Zhang, Z., Karnezi, E., Pandis, S. N., Xie, C., Li, Z., Sun, J., Ma, N., Xu, W., Fu, P., Wang, Z., Zhu, J., Worsnop, D. R., Lee Ng, N. and Sun, Y.: Organic aerosol volatility and viscosity in the North China Plain: Contrast between summer and winter, Atmos. Chem. Phys., 21(7), 5463–5476, doi:10.5194/acp-21-5463-2021, 2021.

Yang, L. H., Takeuchi, M., Chen, Y. and Ng, N. L.: Characterization of thermal decomposition of oxygenated organic compounds in FIGAERO-CIMS, Aerosol Sci. Technol., 55(12), 1321–1342, doi:10.1080/02786826.2021.1945529, 2021.

Yatavelli, R. L. N. and Thornton, J. A.: Particulate Organic Matter Detection Using a Micro-Orifice Volatilization Impactor Coupled to a Chemical Ionization Mass Spectrometer (MOVI-CIMS), Aerosol Sci. Technol., 44(1), 61–74, doi:10.1080/02786820903380233, 2010.

Ye, C., Yuan, B., Lin, Y., Wang, Z., Hu, W., Li, T., Chen, W., Wu, C., Wang, C., Huang, S., Qi, J., Wang, B., Wang, C., Song, W., Wang, X., Zheng, E., Krechmer, J., Ye, P., Zhang, Z., Wang, X., Worsnop, D. and Shao, M.: Chemical

characterization of oxygenated organic compounds in gas-phase and particle-phase using iodide-CIMS with FIGAERO in urban air, Atmos. Chem. Phys., (November), 1–62, doi:10.5194/acp-2020-1187, 2020.

Ye, Q., Wang, M., Hofbauer, V., Stolzenburg, D., Chen, D., Schervish, M., Vogel, A., Mauldin, R. L., Baalbaki, R., Brilke, S., Dada, L., Dias, A., Duplissy, J., El Haddad, I., Finkenzeller, H., Fischer, L., He, X., Kim, C., Kürten, A., Lamkaddam, H., Lee, C. P., Lehtipalo, K., Leiminger, M., Manninen, H. E., Marten, R., Mentler, B., Partoll, E., Petäjä, T., Rissanen, M., Schobesberger, S., Schuchmann, S., Simon, M., Tham, Y. J., Vazquez-Pufleau, M., Wagner, A. C., Wang, Y., Wu, Y., Xiao, M., Baltensperger, U., Curtius, J., Flagan, R., Kirkby, J., Kulmala, M., Volkamer, R., Winkler, P. M., Worsnop, D. and Donahue, N. M.: Molecular Composition and Volatility of Nucleated Particles from α-Pinene Oxidation between -50 °c and +25 °c, Environ. Sci. Technol., 53(21), 12357–12365, doi:10.1021/acs.est.9b03265, 2019.

Ylisirniö, A., Buchholz, A., Mohr, C., Li, Z., Barreira, L., Lambe, A., Faiola, C., Kari, E., Yli-Juuti, T., Nizkorodov, S., Worsnop, D., Virtanen, A. and Schobesberger, S.: Composition and volatility of SOA formed from oxidation of real tree emissions compared to single VOC-systems, Atmos. Chem. Phys. Discuss., (October), 1–29, doi:10.5194/acp-2019-939, 2019.

Ylisirniö, A., Buchholz, A., Mohr, C., Li, Z., Barreira, L., Lambe, A., Faiola, C., Kari, E., Yli-Juuti, T., Nizkorodov, S. A., Worsnop, D. R., Virtanen, A. and Schobesberger, S.: Composition and volatility of secondary organic aerosol (SOA) formed from oxidation of real tree emissions compared to simplified volatile organic compound (VOC) systems, Atmos. Chem. Phys., 20(9), 5629–5644, doi:10.5194/acp-20-5629-2020, 2020.

Ylisirniö, A., Barreira, L. M. F., Pullinen, I., Buchholz, A., Jayne, J., Krechmer, J. E., Worsnop, D. R., Virtanen, A. and Schobesberger, S.: On the calibration of FIGAERO-ToF-CIMS: Importance and impact of calibrant delivery for the particle-phase calibration, Atmos. Meas. Tech., 14(1), 355–367, doi:10.5194/amt-14-355-2021, 2021.

Zhao, Y., Hallar, A. G. and Mazzoleni, L. R.: Atmospheric organic matter in clouds: Exact masses and molecular formula identification using ultrahigh-resolution FT-ICR mass spectrometry, Atmos. Chem. Phys., 13(24), 12343–12362, doi:10.5194/acp-13-12343-2013, 2013.

Zhou, W., Xu, W., Kim, H., Zhang, Q., Fu, P., Worsnop, D. R. and Sun, Y.: A review of aerosol chemistry in Asia: Insights from aerosol mass spectrometer measurements, Environ. Sci. Process. Impacts, 22(8), 1616–1653, doi:10.1039/d0em00212g, 2020.